Fuel 321 (2022) 123987

Contents lists available at ScienceDirect

Fuel

journal homepage: www.elsevier.com/locate/fuel

Full length article

Enhancing the efficiency of power- and biomass-to-liquid fuel processes using fuel-assisted solid oxide electrolysis cells

Anders S. Nielsen [a], M. Ostadi [b], Bjørn Austbø [c], M. Hillestad [b], Gonzalo del Alamo [d], Odne Burheim [c,*]

[a] Department of Mechanical and Materials Engineering, Queen's University, 130 Stuart Street, Kingston, ON, K7L 2V9, Canada
[b] Department of Chemical Engineering, Norwegian University of Science and Technology, NO-7491 Trondheim, Norway
[c] Department of Energy and Process Engineering, Norwegian University of Science and Technology, Trondheim, Norway
[d] SINTEF Energy Research, N-7465 Trondheim, Norway

ARTICLE INFO

Keywords:
Power- and biomass-to-liquid fuel
Thermodynamics
Fischer–Tropsch reactor
Liquid synthetic fuel
Solid oxide electrolysis cell
Fuel-assisted electrolysis

ABSTRACT

Power- and biomass-to-liquid fuel processes (PBtL) can utilize renewable energy and residual forestry waste to produce liquid synthetic fuels, which have the potential to mitigate the climate impacts of the current transportation infrastructure, including the long-haul aviation sector. In a previous study, we demonstrated that implementing a solid oxide electrolysis cell (SOEC) in the PBtL process can significantly increase the energy efficiency of fuel production, by supplying the produced hydrogen to a reverse water gas shift (RWGS) reactor to generate syngas, which is then fed downstream to a Fischer–Tropsch (FT) reactor. The tail gas emitted from the FT reactor consists primarily of a mixture of hydrogen, carbon monoxide, and methane, and is often recycled to the entrained flow gasifier located at the beginning of the process. In this analysis, we investigate the efficiency gains of the PBtL process as a result of redirecting the tail gas of the FT reactor to the anode of an SOEC to serve as fuel. Supplying fuel to an SOEC can lower the electrical work input required to facilitate steam electrolysis when reacting electrochemically with oxide ions in the anode, which in turn can reduce oxygen partial pressures and thus alleviate material degradation. Accordingly, we develop a thermodynamic framework to reveal the performance limits of fuel-assisted SOECs (FASOECs) and provide strategies to minimize oxygen partial pressures in the SOEC anode. Additionally, we elucidate how much fuel is required to match the heating demands of a cell when steam is supplied to the cathode over a broad range of inlet temperatures, and demonstrate the influence of a set of reaction pathways of the supplied fuel on the operating potential of an FASOEC and the corresponding efficiency gain of the PBtL process. Based on preliminary calculations, we estimate that implementing an FASOEC in the PBtL process can increase the energy efficiency of fuel production to more than 90%, depending on the amount of FT tail gas available to the system.

1. Introduction

One of the greatest societal challenges that needs to be resolved in the coming years is limiting the global temperature increase to less than 1.5 °C [1]. Such a target requires immense reductions in the exploitation of fossil fuels, a 50% decrease in emissions by the year 2030, and a carbon-neutral energy economy by the year 2050. The aviation sector represents 12% of the emissions produced by the transportation sector, and bio-based fuels hold potential for reducing the emissions from this sector by 80% [2]. This is an important contribution since 80% of the emissions in the aviation sector correspond to long-haul transportation (>1500 km) [2]; a domain in which conversion to fuels with lower volumetric energy densities (batteries and hydrogen) is challenging. For the long-haul aviation sector, promising alternatives to fossil fuels are liquid synthetic fuels, which can be produced using carbon feedstocks that are naturally embedded in preexisting biological cycles, in tandem with hydrogen generated from renewable sources of energy. Several recent reviews [2–9] and research articles [10–33] have addressed this subject, as well as related process concepts. These are processes that can attain high efficiencies, and in fact, a study conducted by Hillestad et al. [34] determined that, when converting forestry waste into liquid fuels using a process involving an entrained flow gasifier, a reverse

* Corresponding author.
E-mail addresses: anders.nielsen@queensu.ca (A.S. Nielsen), mostadi@mit.edu (M. Ostadi), bjorn.austbo@ntnu.no (B. Austbø), magne.hillestad@ntnu.no (M. Hillestad), gonzalo.alamo@sintef.no (G. del Alamo), burheim@ntnu.no (O. Burheim).

https://doi.org/10.1016/j.fuel.2022.123987
Received 10 February 2022; Received in revised form 9 March 2022; Accepted 24 March 2022
Available online 8 April 2022

Nomenclature

Acronyms

BtL	Biomass-to-liquid fuel
FAPBtL	Fuel-assisted power- and biomass-to-liquid fuel
FASOEC	Fuel-assisted solid oxide electrolysis cell
FT	Fischer–Tropsch
PBtL	Power- and biomass-to-liquid fuel
PEM	Polymer electrolyte membrane
RWGS	Reverse water gas shift
SOEC	Solid oxide electrolysis cell
WGS	Water gas shift

Symbols

$\dot{n}$	Component molar flow rate (mol s^{-1})
$\dot{Q}$	Rate of heat transfer (W)
$\dot{q}$	Rate of sensible energy transfer (W)
$\dot{W}$	Rate of work (W)
A^e	Electrolyte in-plane area (cm^2)
E	Potential (V)
F	Faraday constant (C mol^{-1})
g	Gibbs free energy (J mol^{-1})
h	Molar enthalpy (J mol^{-1})
I	Current (A)
i	Current density (A cm^{-2})
R	Ideal gas constant (J mol^{-1} K^{-1})
R^e	Electrolyte ionic resistance (Ω)
R_{ASR}	Area-specific resistance (Ω cm^2)
s	Molar entropy (J mol^{-1} K^{-1})
T	Temperature (K)
U_{H_2O}	Steam utilization factor (-)
V	Overpotential (V)
x	Component molar fraction (-)
z	Number of electrons transferred (-)

Greek Letters

δ^e	Electrolyte thickness (μm)
Δ_r	Change of reaction (-)
$\Delta_{in\text{-}out}$	Change between inlet and outlet (-)
$\dot{\wp}_s$	Rate of entropy generation (W K^{-1})
σ^e	Electrolyte ionic conductivity (S cm^{-1})
ζ	Ratio of fuel supplied to hydrogen produced (-)

Superscripts

∘	Standard state conditions
ν	Stoichiometric coefficient
a	Anode
c	Cathode
$cell$	Cell
e	Electrolyte
in	Inlet
out	Outlet
rev	Reversible
tn	Thermoneutral

Subscripts

CH_4	Methane
CO	Carbon monoxide
CO_2	Carbon dioxide
H_2	Hydrogen
H_2O	Steam
O_2	Oxygen
$comb$	Combustion reaction pathway
$elec$	Electrochemical reaction pathway
i	Oxidation reaction index
lc	Limiting case
max	Maximum
mix	Fuel mixture

water gas shift (RWGS) reactor, and a Fischer–Tropsch (FT) reactor (*i.e.* biomass-to-liquid fuel (BtL) process), the fuel output per input biomass can be more than doubled by supplying hydrogen to the RWGS reactor. This process is referred to as power- and biomass-to-liquid fuel (PBtL). The BtL process has a carbon utilization efficiency of 35%–40% and an energy efficiency of 50%–55%. When PBtL is performed using an SOEC under adiabatic and isothermal conditions (*i.e.* at the thermoneutral potential), the ratio between the electrical work input and the extra liquid fuel output becomes ~1.2. Further improvement, such that the electrical work input can be converted almost directly into fuel (~10 kWh/L_{fuel}), can be obtained using residual heat from the entrained flow gasifier to compensate for the reversible heat demands of the electrolysis cell at elevated temperatures (*i.e.* operating the cell near the reversible potential). These examples demonstrate the advantages of implementing SOECs in a BtL process in order to generate liquid synthetic fuels in a sustainable and renewable manner, since PBtL has a carbon utilization efficiency of more than 90% and an energy efficiency of 65%–75%, depending on the heat utilization of the entrained flow gasifier. Most studies and reviews in the literature have acknowledged the benefits of increased carbon utilization by adding hydrogen to the BtL process: some of which have recognized the advantages of using SOECs over low-temperature electrolysis technologies to attain increased efficiencies [35–37], while many others have realized the potential to exploit the chemical energy of the tail gas by feeding it to a biomass gasifier. One such study had suggested to supply the tail gas to a turbine for power generation; however, doing so would consequently lower the carbon efficiency, since the combustion process would emit carbon in the form of carbon dioxide. Accordingly, we propose feeding the tail gas to the anode of an SOEC to reduce the energy demands of the PBtL process, while retaining a high carbon efficiency. To the best of the authors' knowledge, this approach has yet to be investigated in the literature and presents a compelling alternative for the utilization of tail gas in order to enhance the efficiency of the PBtL process, as well as other similar processes.

1.1. Biomass-to-liquid fuel - BtL

In the simplest way, BtL can be described as burning wood or other biomass with pure oxygen in an understoichiometric amount to create syngas. This syngas is subsequently fed to an FT reactor to produce hydrocarbon chains ranging primarily from pentane and upwards in length. This gasifying process typically uses forestry waste that has been ground into small granulates, which are then dried and delivered to an entrained flow gasifier, where pure oxygen is fed understoichiometrically to produce syngas. However, the resultant gases contain less hydrogen than desired for producing hydrocarbon chains. Steam is therefore added to convert carbon monoxide into hydrogen and carbon dioxide within a water gas shift (WGS) reactor. An additional challenge arises from the syngas exiting the gasifier at too high a temperature (1200–1600 °C) for what is desirable in the WGS reactor. Some of this

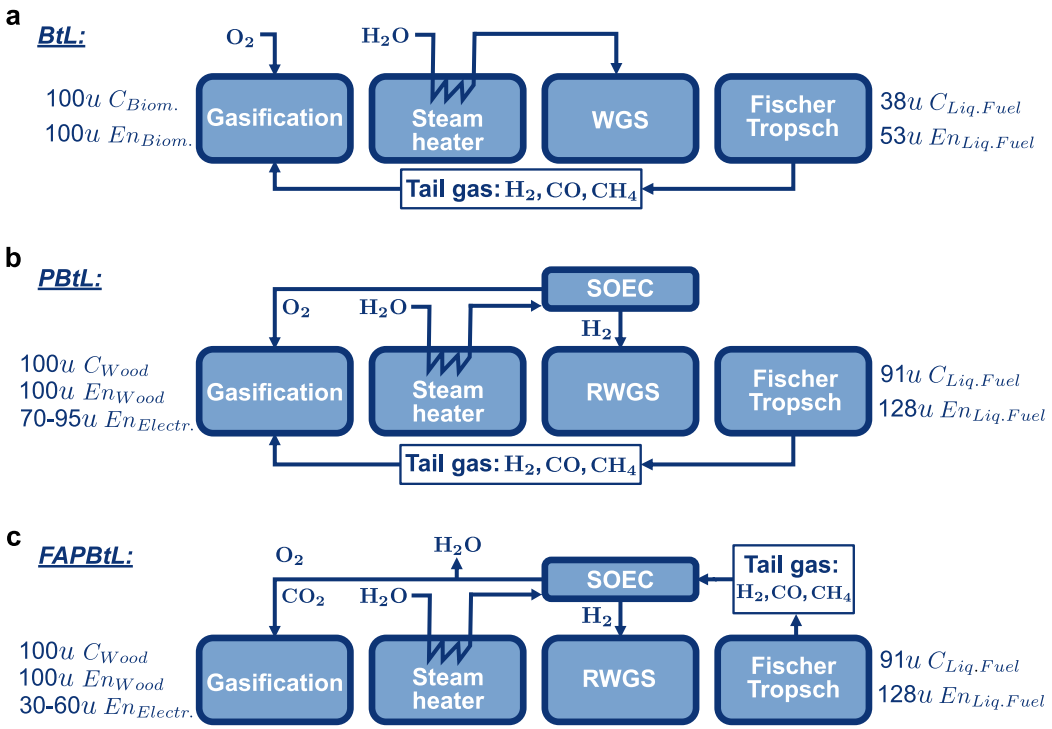

Fig. 1. Simplified schematic of the (a) BtL, (b) PBtL, and (c) FAPBtL processes, alongside relative input and output rates of energy, En_i, and carbon mass, C_i, for the complete processes.

heat is consequently used to produce steam, which then enters the WGS reactor alongside syngas from the gasifier.

BtL is a medium-efficient process in which more than half the energy embedded in the biomass is transferred to the fuel. However, the process utilizes only 35%–40% of the carbon in the biomass, resulting in the emission of carbon dioxide from the FT reactor. A simplified overview of the BtL process, as well as the corresponding energy and carbon balances, are illustrated in Fig. 1(a).

1.2. Power- and biomass-to-liquid fuel - PBtL

Since BtL has more than twice the amount of carbon than it can utilize in hydrocarbon production, adding hydrogen in place of steam would shift the process towards producing less carbon dioxide and more hydrocarbons. This hydrogen can be derived from virtually any source, but high-temperature electrolysis in the form of SOECs is energetically favourable in comparison to low-temperature technologies, including alkaline and polymer electrolyte membrane (PEM) electrolysis cells. In fact, at temperatures between 700–900 °C, SOECs use only 33–35 kWh $kg_{H_2}^{-1}$, whereas alkaline and PEM electrolysis cells use approximately 50–60 kWh $kg_{H_2}^{-1}$, depending on the operating conditions [38] (see Refs. [39,40] for comparisons of operating potentials and current densities of each technology). When using a portion of the waste heat from the gasifier to superheat the steam before it enters an SOEC, its energy demand can drop to as low as 25–28 kWh $kg_{H_2}^{-1}$, which is roughly half the electrical energy needed in comparison to low-temperature technologies.

Introducing an SOEC and electrical power to the BtL process makes it a power- and biomass-to-liquid fuel (PBtL) process. Rather than supplying steam to produce hydrogen *via* WGS, hydrogen produced in an SOEC is fed downstream alongside carbon dioxide to yield carbon monoxide and steam from the reverse water gas shift (RWGS) reaction. Only a fraction of the hydrogen is converted into steam, resulting in an enriched mixture of carbon monoxide and hydrogen that exit the RWGS reactor, which therefore enhances the production rate of hydrocarbons using FT reactors and limits the emission of carbon dioxide. There are two central advantages of the PBtL process in comparison to BtL: firstly, more than 90% of the carbon is utilized for fuel production in PBtL, which is a dramatic improvement in comparison to BtL. Secondly, the electrical energy input is close to parity with respect to the energy embedded in the additional fuel using superheated steam and the PBtL process. Comparisons between BtL and PBtL, as well as their carbon and energy balances, are shown in Fig. 1(a) and (b), respectively.

1.3. Fuel-assisted PBtL - FAPBtL

The simplified process diagrams shown in Fig. 1(a) and (b) illustrate another opportunity to further improve the efficiency of the PBtL process, which involves an alternative use of the tail gas emitted from the FT reactor. This tail gas consists primarily of a mixture of hydrogen, carbon monoxide, and methane, as well as trace amounts of lighter hydrocarbons. In the BtL and PBtL processes, tail gas is fed back into the gasifier with a stream of oxygen to combust the supplied biomass. The tail gas is thus utilized to improve carbon and energy efficiency, while oxygen is added to gasify the tail gas and biomass into a syngas mixture. However, this tail gas contains energy that can be used to supplement the energy demands of hydrogen production, which is accomplished by delivering the tail gas to the anode of an SOEC, as shown in Fig. 1(c). In doing so, the free energy of the tail gas mixture corresponding to the combustion reaction in the gasifier is used to reduce the electrical work input required to produce hydrogen in an SOEC. In certain cases, the electrical energy input of the PBtL process can be reduced by a factor of two, meaning that the produced fuel possesses more energy than the amount of electricity supplied to the system. This does not suggest that the energy efficiency exceeds 100%, but rather indicates that the energy embedded in the forestry waste is used more effectively and can result in an overall energy efficiency between 80%–95% (*i.e.* electrical and biomass input to fuel output), depending on whether the steam supplied to the cathode is delivered at an inlet temperature above the operating temperature of an SOEC. It is assumed that the tail gas emitted by the FASOEC anode is directed to the entrained flow gasifier, as shown in Fig. 1(c), but does not have an influence on the results found in the

current study. A detailed process model would be required to compare the potential benefits of feeding the FASOEC anode tail gas to either the entrained flow gasifier or the FT reactor.

1.4. Solid oxide electrolysis cells - SOECs

SOECs are often used to electrochemically reduce an inlet feed of steam or carbon dioxide into an outlet stream of hydrogen or carbon monoxide [39]. In this analysis, we are interested in hydrogen production and thus restrict the current study to consider only steam electrolysis. Fig. 2(a) illustrates the operating principle of a steam-fed SOEC.

The thermodynamics of an SOEC are such that the minimum energy required is the reaction enthalpy $\Delta_r h$. This is the sum of reversible heat $T\Delta_r s$ and reversible work $\Delta_r g$, and a cell is typically operated in such a way that the Ohmic heat produced by the transport of oxide ions across the electrolyte is as large as the reversible heat, so that the electrical energy input is equal to the reaction enthalpy (*i.e.* $\Delta_r h = \Delta_r g + T\Delta_r s \rightarrow E^{tn} = E^{rev} + IR^e$) [38]. The reason for operating a cell at thermoneutral potential E^{tn} is that Ohmic losses IR^e increase with decreasing temperature, and when the operating temperature is too low with increased Ohmic heat generation rates (*i.e.* above the minimum energy demand), the cell will self-heat to a temperature at which the Ohmic heat is balanced with the entropic heat requirements of the electrolysis reaction. When the current density decreases, however, the Ohmic heat can be lower than the entropic heat demand, and the cell will self-cool to a temperature at which the Ohmic resistance increases, and the thermoneutral potential will be reached again. Furthermore, it is possible to supply steam to the cathode at a temperature higher than the operating temperature of a cell, which will result in a temperature increase of the cell and Ohmic heating will be reduced. In doing so, the entropic heat demand is provided by a combination of the Ohmic heat from the electrolyte and the sensible heat from the superheated steam entering the cathode. This is challenging for at least two reasons: firstly, it can impose high temperature gradients within a cell, leading to thermal expansion of the materials and subsequently increased material degradation. Secondly, the inlet steam might need to be supplied at an extremely high temperature in order to provide sufficient amounts of thermal energy to compensate for the reduced Ohmic heating and the entropic heat demands of electrolysis. Both of these challenges can be overcome by staging SOECs in series, which reheats the steam and the product hydrogen between stages [33]. For example, if it is desirable to utilize 20% of the incoming steam at each stage while using a total of five SOECs in series, the inlet steam after each stage would require decreasing amounts of heat. Such a setup would require five heat exchangers for the gases (one for 100% steam, a second for 80% steam and 20% hydrogen, and so forth), and from the perspective of process design, considering both capital expenditures and operational challenges with respect to thermal gradients, staging SOECs in series is expected to be undesirable. However, exploiting the thermal energy embedded in the tail gas of the FT reactor, by redirecting it to the anode of an SOEC, presents an opportunity to alleviate thermal gradients within a cell, thus promoting the feasibility to perform steam electrolysis in stages.

1.5. Fuel-assisted SOECs - FASOECs

As mentioned above, the minimum amount of work input required to facilitate the electrochemical reduction of steam corresponds to the Gibbs free energy, $\Delta_r g$, and can be expressed in terms of a potential according to: $\Delta_r g = -nFE^{rev}$. However, if hydrogen is fed to the anode of an SOEC at the same rate at which it is produced in the cathode, the cell would therefore operate as a hydrogen pump, wherein hydrogen is transferred from the anode to the cathode. In this instance, the supply of hydrogen to the anode represents an energy input which balances the amount of energy needed to produce hydrogen in the cathode. In this respect, the hydrogen supplied to the anode as fuel will thus lower the energy demands for producing hydrogen in an SOEC, and is therefore referred to as a fuel-assisted SOEC (FASOEC). The delivered hydrogen can be replaced or supplemented with a mixture of various types of fuels, including carbon monoxide, methane, higher-order hydrocarbons, as well as ammonia. In this paper, we examine the thermodynamics of an FASOEC with an inlet fuel mixture of hydrogen, carbon monoxide, and methane, as illustrated in Fig. 2(b), since this composition is found in the tail gas of FT reactors in the PBtL process [34]. It should be noted that the oxidation of fuel in the anode has the potential to cause issues in terms of managing thermal gradients and stresses within a cell, and we therefore develop strategies to appropriately select the inlet molar flow rate of fuel in order to operate a cell at a desired temperature.

1.6. Efforts in FASOECs

The concept of supplying fuel to the anode of an SOEC was introduced in a patent developed by Pham et al. [41], which demonstrated a 50% reduction in operating potential when using methane as the reducing gas. The addition of fuel has also been exploited in later studies, with reported decreases in operating potential by as much as one order of magnitude [42,43], while Tao et al. [44] revealed the capacity of these devices to co-generate electricity and hydrogen. Materials characterization studies have also been conducted to evaluate the performance and stability of a variety of electrodes by subjecting them to different fuels, including hydrogen, carbon monoxide, and methane [45–47]. Other experiments were performed to elucidate the influence of fuel utilization on the operating potential of hydrogen- [48] and methane-assisted [49] electrolysis cells. The former determined that supplying an insufficient amount of hydrogen can negate the benefits of operating in fuel-assisted mode, thus illustrating the importance of controlling the rate at which fuel is delivered to the cell; the latter concluded the electro-oxidation of hydrogen governs performance at high methane conversion ratios, whereas the direct oxidation of methane dominates at lower ratios. While the previous studies have made important contributions to the design and development of FASOECs and have highlighted the ability to significantly reduce electricity consumption, it is still not understood how the reaction pathway of the supplied fuel – either electrochemical or chemical – influences the performance limits of these devices.

A limited number of theoretical analyses have also been performed to elucidate the benefits of fuel-assisted electrolysis and to quantify mass and momentum transport, as well as chemical and electrochemical reaction rates. In the latter portion of the study conducted by Martinez-Frias et al. [42], a thermodynamic analysis of a coupled natural gas-assisted SOEC and heat recovery system determined that efficiencies of up to 90% could be attained, based on the total energy supplied to the cell. Computational studies of direct carbon [50] and methane-assisted [51,52] SOECs have also been undertaken to evaluate the effects of various operating conditions and design specifications on cell performance, such as electrode thickness, operating temperature and pressure, inlet molar fraction, and flow velocity. Another study compared the efficiency of carbon monoxide- and methane-assisted electrolyzers to conventional cells, and demonstrated that utilizing either fuel results in greater efficiencies than the latter, with methane-assisted producing the highest values due to the elevated mixtures of hydrogen and carbon monoxide generated by steam reforming [53]. Numerical models of combined FASOECs and FT reactors have shown that the operating potential and temperature of a cell can have a significant impact on the composition of products generated by the FT system [54,55]. The theoretical models developed in these studies have been integral to the advancement of FASOECs, revealing important information concerning the impacts of various design parameters on their performance. Despite these efforts, however, an understanding of how much fuel is required to minimize oxygen partial pressures in the anode and to heat an inlet flow of steam to the operating temperature of

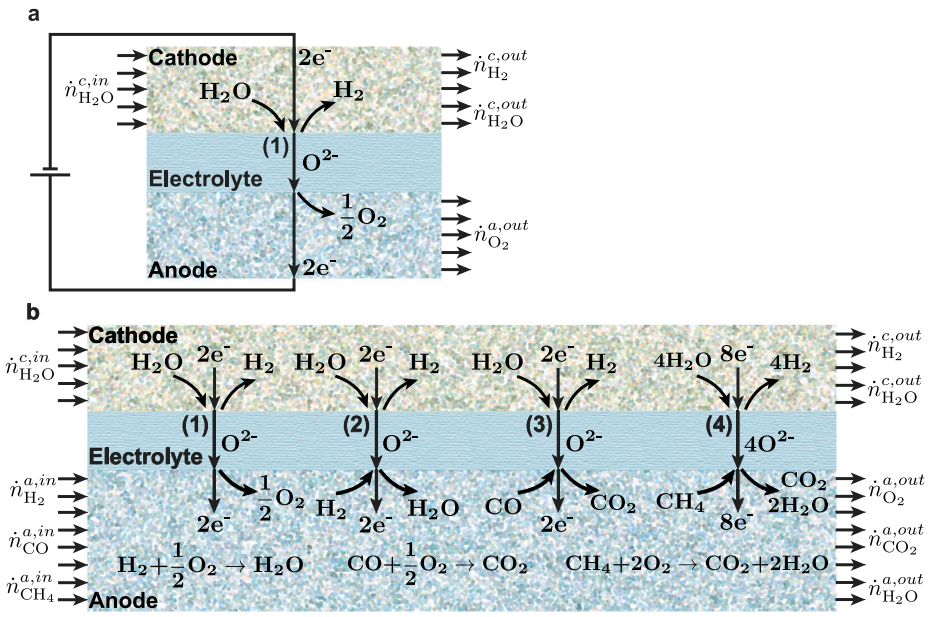

Fig. 2. (a) Schematic of a solid oxide electrolysis cell (SOEC) in which steam is electrochemically reduced to produce hydrogen and oxide ions, and oxygen proceeds to evolve in the anode. (b) Schematic of a fuel-assisted solid oxide electrolysis cell (FASOEC), wherein a mixture of hydrogen, carbon monoxide, and methane is supplied to the anode. The electrochemical reactions in the anode considered in this analysis are: (1) oxygen evolution, (2) hydrogen oxidation, (3) carbon monoxide oxidation, and (4) complete oxidation of methane. The chemical reactions considered in the anode are the combustion of hydrogen, carbon monoxide, and methane.

a cell remains unclear. Therefore, a thermodynamic analysis is needed in order to address the aforementioned items, as well as to reveal the operating limits of FASOECs for a particular reaction pathway of the supplied fuel.

1.7. Objective and outline

In this study, we develop a thermodynamic framework to explore the performance limits of FASOECs when tail gas from an FT reactor in the PBtL process is supplied to the anode. This tail gas consists of a mixture of hydrogen (57%), carbon monoxide (29%), and methane (14%), and because the pathways by which each component reacts in the anode is unclear (*i.e.* electrochemical or chemical), we examine five possible limiting cases, which are as follows: (*i*) all components react *via* combustion, (*ii*) hydrogen reacts electrochemically with the remaining components reacting *via* combustion, (*iii*) carbon monoxide reacts electrochemically with the remaining components reacting *via* combustion, (*iv*) methane reacts electrochemically with the remaining components reacting *via* combustion, and (*v*) all components react electrochemically. For each of these cases, we reveal how a given reaction pathway influences the operating potential required to facilitate steam electrolysis, as well as the flow rate of fuel needed to heat an inlet flow of steam to the operating temperature of a cell. Additionally, we provide strategies to minimize oxygen partial pressures in the anode using the tail gas from an FT reactor, which can inhibit material degradation and improve the longevity of these devices. It is found that the reductions in operating potential of an FASOEC can increase the energy efficiency of fuel production of the PBtL process to more than 90%. As a result of this study, designers will be able to select an appropriate flow rate of fuel in order to attain a desired reduction in operating potential and to heat an inlet supply of steam to a particular cell operating temperature.

2. Thermodynamic framework

In an SOEC, steam is delivered to the cathode at a molar flow rate of $\dot{n}^{c,in}_{H_2O}$, where it is then electrochemically reduced at the triple phase boundaries to produce oxide ions and hydrogen gas, as illustrated in Fig. 2(a). The corresponding half-cell reaction is denoted by:

$$H_2O + 2e^- \rightarrow H_2 + O^{2-}. \tag{1}$$

Subsequently, the produced hydrogen gas and unused steam exit the cathode at molar flow rates $\dot{n}^{c,out}_{H_2}$ and $\dot{n}^{c,out}_{H_2O}$, respectively, while oxide ions migrate through the electrolyte towards the triple phase boundaries in the anode, where the oxygen evolution reaction occurs to form oxygen gas. The half-cell reaction in the anode is therefore written as:

$$O^{2-} \rightarrow \frac{1}{2}O_2 + 2e^-, \tag{2}$$

and the overall reaction is given by:

$$H_2O \rightarrow H_2 + \frac{1}{2}O_2. \tag{3}$$

When operating in fuel-assisted mode, the half-cell reaction in the cathode remains as described above for this analysis, while hydrogen, carbon monoxide, and methane are supplied to the anode at molar flow rates $\dot{n}^{a,in}_{H_2}$, $\dot{n}^{a,in}_{CO}$, and $\dot{n}^{a,in}_{CH_4}$, respectively. Each component can react electrochemically with oxide ions at the triple phase boundaries or chemically with the evolved oxygen gas in the anode, as shown in Fig. 2(b). We assume that the chemical/electrochemical oxidation of hydrogen, carbon monoxide, and methane are the only reactions that occur in the anode, thus yielding outlet molar flow rates of oxygen, $\dot{n}^{a,out}_{O_2}$, carbon dioxide, $\dot{n}^{a,out}_{CO_2}$, and steam, $\dot{n}^{a,out}_{H_2O}$. In reality, there may also be water gas shift and methane steam reforming reactions occurring in the anode due to a mixture of hydrogen, carbon monoxide, methane, carbon dioxide, and steam in the presence of a catalyst, but are neglected for the sake of this analysis. It is important to note that there is a critical distinction between chemical and electrochemical reaction pathways; the former generates thermal energy that becomes available to the cell as a result of the enthalpy change of combustion, while the latter yields the entropic component of the reaction as thermal energy, with the remaining Gibbs free energy of the reaction (*i.e.* $\Delta_r h_i = \Delta_r g_i + T\Delta_r s_i$) serving as work to reduce the potential required to facilitate electrolysis. It is important to note that the electrochemical oxidation of a particular fuel still generates heat that is proportional to the entropy change of said reaction (*i.e.* $T\Delta_r s_i$). A numerical approach to quantify

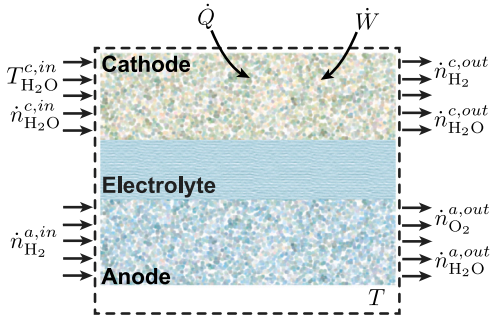

Fig. 3. Schematic of the control volume for the presented thermodynamic analysis. All inlet and outlet parameters are evaluated at operating temperature, T, except for the inlet flow of steam in the cathode, which is evaluated at inlet temperature $T_{H_2O}^{c,in}$.

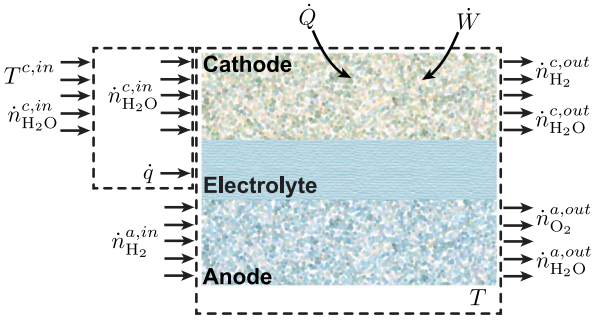

Fig. 4. Schematic of the modified control volume of the presented thermodynamic analysis, assuming the sensible energy difference between the inlet steam and FASOEC is converted to thermal energy without extracting work.

the partitioning between chemical and electrochemical reaction pathways in FASOECs has been developed to compliment this analysis, and is undertaken as a separate study since it lies outside the scope of the current work.

2.1. Thermodynamic analysis

We begin by developing a thermodynamic model of an FASOEC with steam and hydrogen supplied to the cathode and anode, respectively, at molar flow rates $\dot{n}_{H_2O}^{c,in}$ and $\dot{n}_{H_2}^{a,in}$, as shown in Fig. 3. Steam is supplied at inlet temperature $T_{H_2O}^{c,in}$, while the rest of the operating parameters within and delivered to the control volume are evaluated at temperature T. Assuming a steady state, steady flow system and complete electrochemical utilization of hydrogen fuel, the first law of thermodynamics for the cell is expressed as:

$$\dot{W} + \dot{Q} + \dot{n}_{H_2O}^{c,in} h_{H_2O}^{c,in} + \dot{n}_{H_2}^{a,in} h_{H_2}^{a,in} = \dot{n}_{H_2}^{c,out} h_{H_2}^{c,out} + \dot{n}_{H_2O}^{c,out} h_{H_2O}^{c,out} + \dot{n}_{O_2}^{a,out} h_{O_2}^{a,out} + \dot{n}_{H_2O}^{a,out} h_{H_2O}^{a,out}, \quad (4)$$

where $\dot{W}$ is the rate of work, $\dot{Q}$ is the heat transfer rate, and h is the molar enthalpy of each component evaluated at either the inlet or outlet of the cell. Substituting molar balances: $\dot{n}_{H_2}^{c,out} = U_{H_2O}\dot{n}_{H_2O}^{c,in}$; $\dot{n}_{H_2O}^{c,out} = (1 - U_{H_2O})\dot{n}_{H_2O}^{c,in}$; $\dot{n}_{O_2}^{a,out} = (U_{H_2O}\dot{n}_{H_2O}^{c,in} - \dot{n}_{H_2}^{a,in})/2$; and $\dot{n}_{H_2O}^{a,out} = \dot{n}_{H_2}^{a,in}$ into Eq. (4) yields:

$$\dot{W} + \dot{Q} + \dot{n}_{H_2O}^{c,in} \Delta_{in\text{-}out} h_{H_2O} = U_{H_2O}\dot{n}_{H_2O}^{c,in}\left(\Delta_r h_{H_2O} + \zeta_{H_2}\Delta_r h_{H_2}\right), \quad (5)$$

where $\Delta_{in\text{-}out} h_{H_2O}$ denotes the change in molar enthalpy of steam between the inlet and outlet, $\Delta_r h_i$ is the enthalpy change of reaction i, U_{H_2O} is the utilization factor of steam, and ζ_{H_2} is the molar flow rate of hydrogen supplied to the anode in reference to the molar flow rate of hydrogen produced in the cathode (*i.e.* $\zeta_{H_2} = \dot{n}_{H_2}^{a,in}/U_{H_2O}\dot{n}_{H_2O}^{c,in}$). Applying the second law of thermodynamics to the system illustrated in Fig. 3 produces the following entropy balance:

$$\dot{n}_{H_2O}^{c,in} s_{H_2O}^{c,in} + \dot{n}_{H_2}^{a,in} s_{H_2}^{a,in} - \left(\dot{n}_{H_2}^{c,out} s_{H_2}^{c,out} + \dot{n}_{H_2O}^{c,out} s_{H_2O}^{c,out} + \dot{n}_{O_2}^{a,out} s_{O_2}^{a,out} + \dot{n}_{H_2O}^{a,out} s_{H_2O}^{a,out}\right) + \frac{\dot{Q}}{T} + \dot{\wp}_s = 0. \quad (6)$$

where s is the molar entropy of each component, evaluated at the inlet or outlet of the cell, and $\dot{\wp}_s$ is the rate of entropy generation in the system due to irreversibilities. Substituting the above definitions of the outlet molar flow rates into Eq. (6) and rearranging for heat transfer rate $\dot{Q}$ yields:

$$\dot{Q} = U_{H_2O}\dot{n}_{H_2O}^{c,in}\left(T\Delta_r s_{H_2O} + \zeta_{H_2} T\Delta_r s_{H_2}\right) - \dot{n}_{H_2O}^{c,in} T\Delta_{in\text{-}out} s_{H_2O} - T\dot{\wp}_s, \quad (7)$$

where $\Delta_r s_i$ is the molar entropy change of reaction i. Finally, upon substitution of Eq. (7) into Eq. (5) and using the definition of the Gibbs free energy (*i.e.* $\Delta_r g_i = \Delta_r h_i - T\Delta_r s_i$), the rate of work crossing the system boundary is expressed as:

$$\dot{W} = U_{H_2O}\dot{n}_{H_2O}^{c,in}\left(\Delta_r g_{H_2O} + \zeta_{H_2}\Delta_r g_{H_2}\right) + T\dot{\wp}_s - \dot{n}_{H_2O}^{c,in}\left(\Delta_{in\text{-}out} h_{H_2O} - T\Delta_{in\text{-}out} s_{H_2O}\right). \quad (8)$$

Eqs. (7) and (8) represent the most general form of the rate of heat and work crossing the system boundary for an FASOEC with steam supplied to the cathode at a different temperature than the rest of the system. Care must be taken to ensure that the rate of entropy production is always positive when simplifying Eqs. (7) and (8), due to the terms with the $\Delta_{in\text{-}out}$ prefix.

2.2. Reversible FASOEC and minimum work input

The reversible potential represents the minimum amount of work supplied to a cell in order to facilitate electrolysis. For a reversible process, the rate of entropy production is zero (*i.e.* $\dot{\wp}_s = 0$), and the reversible work of an FASOEC is simplified to:

$$\dot{W}^{rev} = U_{H_2O}\dot{n}_{H_2O}^{c,in}\left(\Delta_r g_{H_2O} + \zeta_{H_2}\Delta_r g_{H_2}\right) - \dot{n}_{H_2O}^{c,in}\left(\Delta_{in\text{-}out} h_{H_2O} - T\Delta_{in\text{-}out} s_{H_2O}\right). \quad (9)$$

Assuming that sensible energy $\dot{n}_{H_2O}^{c,in}(\Delta_{in\text{-}out} h_{H_2O} - T\Delta_{in\text{-}out} s_{H_2O})$ is transferred to the cell as thermal energy without extracting any work, as illustrated in Fig. 4, the rate of reversible work is thus written as:

$$\dot{W}^{rev} = \dot{n}_{H_2O}^{c,in} U_{H_2O}\left(\Delta_r g_{H_2O} + \zeta_{H_2}\Delta_r g_{H_2}\right), \quad (10)$$

and the rate of heat transfer is expressed as:

$$\dot{Q} = \dot{n}_{H_2O}^{c,in} U_{H_2O}\left(T\Delta_r s_{H_2O} + \zeta_{H_2} T\Delta_r s_{H_2}\right) - \dot{q}, \quad (11)$$

where $\dot{q} = \dot{n}_{H_2O}^{c,in}\Delta_{in\text{-}out} h_{H_2O}$. In instances when it is desirable to provide the amount of energy required to heat the inlet flow of steam to the operating temperature of a cell and to supplement the entropy change of the electrolysis reaction, the inlet molar flow rate of hydrogen must be sufficiently high such that $\dot{Q} = 0$, which results in:

$$\zeta_{H_2} = \frac{\Delta_{in\text{-}out} h_{H_2O} - U_{H_2O} T\Delta_r s_{H_2O}}{U_{H_2O} T\Delta_r s_{H_2}}. \quad (12)$$

A practical way to conceptualize ζ_i is to consider it as the ratio between the molar flow rate of fuel supplied to the anode and the molar flow rate of hydrogen produced in the cathode. For instance, when $\zeta_i = 0$, no fuel is supplied to the anode and the cell behaves as a conventional SOEC; when $\zeta_i = 1$, the amount of fuel delivered is at parity with the amount of hydrogen generated in the cathode. In cases when $\zeta_i > 1$, the added fuel behaves both as a sweep gas and fuel. These statements are valid for single-component fuels and arbitrary fuel mixtures supplied to the anode.

Since the rate of reversible work of a cell is $\dot{W}^{rev} = IE^{rev}$ and current I is given by $I = 2FU_{H_2O}\dot{n}^{c,in}_{H_2O}$, the reversible potential of an FASOEC with pure hydrogen supplied to the anode is expressed as:

$$E^{rev}_{H_2} = \frac{\Delta_r g_{H_2O} + \zeta_{H_2}\Delta_r g_{H_2}}{2F}, \tag{13}$$

where the energy required to facilitate steam electrolysis, $\Delta_r g_{H_2O}$, is written as:

$$\Delta_r g_{H_2O} = \Delta_r g^{\circ}_{H_2O}(T) + RT\ln\left(\frac{x^{c,out}_{H_2}\left(x^{a,out}_{O_2}\right)^{1/2}}{x^{c,in}_{H_2O}}\right), \tag{14}$$

and the Gibbs free energy exploited as a result of the electro-oxidation of hydrogen, $\Delta_r g_{H_2}$, is given by:

$$\Delta_r g_{H_2} = \Delta_r g^{\circ}_{H_2}(T) + RT\ln\left(\frac{x^{a,out}_{H_2O}}{x^{a,in}_{H_2}\left(x^{a,out}_{O_2}\right)^{1/2}}\right), \tag{15}$$

where x_i denotes the molar fraction of each component, evaluated at either the inlet or outlet of the cell, and $\Delta_r g_i^{\circ}(T)$ is the standard state Gibbs free energy of reaction i at temperature T. The outlet molar fraction of oxygen and steam in Eq. (15) are determined using:

$$x^{a,out}_{O_2} = \frac{1-\zeta_{H_2}}{1+\zeta_{H_2}}, \tag{16}$$

and:

$$x^{a,out}_{H_2O} = \frac{2\zeta_{H_2}}{1+\zeta_{H_2}}, \tag{17}$$

respectively, which are obtained from molar balances: $\dot{n}^{a,out}_{O_2} = (U_{H_2O}\dot{n}^{c,in}_{H_2O} - \dot{n}^{a,in}_{H_2})/2$; and $\dot{n}^{a,out}_{H_2O} = \dot{n}^{a,in}_{H_2}$. It should be noted that the presented derivation assumes the complete electrochemical utilization of hydrogen in the anode.

Following an identical thermodynamic analysis for a supply of carbon monoxide to the anode, and assuming that no work is extracted from the additional sensible energy from the inlet feed of steam in the cathode, the reversible potential of CO-assisted electrolysis is written as:

$$E^{rev}_{CO} = \frac{\Delta_r g_{H_2O} + \zeta_{CO}\Delta_r g_{CO}}{2F}, \tag{18}$$

where ζ_{CO} is the ratio of the molar flow rate of carbon monoxide supplied to the anode to the molar flow rate of hydrogen produced in the cathode (*i.e.* $\zeta_{CO} = \dot{n}^{a,in}_{CO}/U_{H_2O}\dot{n}^{c,in}_{H_2O}$) and $\Delta_r g_{CO}$ is the Gibbs free energy released due to the electro-oxidation of carbon monoxide, which is expressed as:

$$\Delta_r g_{CO} = \Delta_r g^{\circ}_{CO}(T) + RT\ln\left(\frac{x^{a,out}_{CO_2}}{x^{a,in}_{CO}\left(x^{a,out}_{O_2}\right)^{1/2}}\right). \tag{19}$$

The outlet molar fractions of oxygen and carbon dioxide in Eq. (19) are evaluated using:

$$x^{a,out}_{O_2} = \frac{1-\zeta_{CO}}{1+\zeta_{CO}}, \tag{20}$$

and:

$$x^{a,out}_{CO_2} = \frac{2\zeta_{CO}}{1+\zeta_{CO}}, \tag{21}$$

respectively, which are derived from molar balances: $\dot{n}^{a,out}_{O_2} = (U_{H_2O}\dot{n}^{c,in}_{H_2O} - \dot{n}^{a,in}_{CO})/2$; and $\dot{n}^{a,out}_{CO_2} = \dot{n}^{a,in}_{CO}$. Similarly, when methane is supplied to the anode, the corresponding reversible potential is expressed according to:

$$E^{rev}_{CH_4} = \frac{4\Delta_r g_{H_2O} + \zeta_{CH_4}\Delta_r g_{CH_4}}{8F}, \tag{22}$$

where $\zeta_{CH_4} = \dot{n}^{a,in}_{CH_4}/U_{H_2O}\dot{n}^{c,in}_{H_2O}$, and the Gibbs free energy released during the complete electro-oxidation of methane is written as:

$$\Delta_r g_{CH_4} = \Delta_r g^{\circ}_{CH_4}(T) + RT\ln\left(\frac{x^{a,out}_{CO_2}\left(x^{a,out}_{H_2O}\right)^2}{x^{a,in}_{CH_4}\left(x^{a,out}_{O_2}\right)^2}\right), \tag{23}$$

where $\Delta_r g^{\circ}_{CH_4}$ is the standard state Gibbs free energy evaluated at temperature T. The outlet molar fraction of oxygen, steam, and carbon dioxide in the anode are denoted by:

$$x^{a,out}_{O_2} = \frac{1-4\zeta_{CH_4}}{1+2\zeta_{CH_4}}, \tag{24}$$

$$x^{a,out}_{H_2O} = \frac{4\zeta_{CH_4}}{1+2\zeta_{CH_4}}, \tag{25}$$

and:

$$x^{a,out}_{CO_2} = \frac{2\zeta_{CH_4}}{1+2\zeta_{CH_4}}, \tag{26}$$

respectively, which are obtained from the following molar balances in the anode: $\dot{n}^{a,out}_{O_2} = U_{H_2O}\dot{n}^{c,in}_{H_2O}/2 - 2\dot{n}^{a,in}_{CH_4}$; $\dot{n}^{a,out}_{H_2O} = 2\dot{n}^{a,in}_{CH_4}$; and $\dot{n}^{a,out}_{CO_2} = \dot{n}^{a,in}_{CH_4}$.

When an arbitrary fuel composition is delivered to the anode of an FASOEC, it is useful to compute the molar flow rate required to heat the inlet flow of steam to operating temperature T and the corresponding reversible potential when the fuel reacts in a purely electrochemical manner. Using the methodology described above, the ratio of the molar flow rate of the fuel mixture to the molar flow rate of hydrogen produced that is necessary to perform electrolysis at the desired temperature and to supplement the entropy change of said reaction is given by:

$$\zeta_{mix,elec} = \frac{\Delta_{in\text{-}out}h_{H_2O} - U_{H_2O}T\Delta_r s_{H_2O}}{U_{H_2O}\sum_i x^{a,in}_i T\Delta_r s_i}, \tag{27}$$

where $\zeta_{mix,elec} = \dot{n}^{a,in}_{mix}/U_{H_2O}\dot{n}^{c,in}_{H_2O}$, and the reversible potential is expressed according to:

$$E^{rev}_{mix,elec} = \frac{(z_{max}/2)\Delta_r g_{H_2O} + \zeta_{mix,elec}\sum_i (z_{max}/z_i)x^{a,in}_i \Delta_r g_i}{z_{max}F}. \tag{28}$$

In Eqs. (27) and (28), the summation terms are evaluated over the number of oxidation reactions i, $x^{a,in}_i$ is the anode inlet molar fraction of the fuel component involved in reaction i, z_i is the number of electrons transferred, and z_{max} is the highest number of electrons transferred in any of the electrochemical reactions considered.

In order to determine the Gibbs free energy of a given reaction at non-standard conditions, it is important to evaluate the terms using compositions at points where streams cross the surfaces of the control volume. The Gibbs free energy of steam electrolysis is still computed using Eq. (14), while the free energy corresponding to each oxidation reaction is evaluated using:

$$\Delta_r g_i = \Delta_r g_i^{\circ}(T) + RT\ln\left(\frac{\prod_{prod} x_l^{\nu_l}}{\prod_{react} x_k^{\nu_k}}\right), \tag{29}$$

where ν is the stoichiometric coefficient of a given component. It should be noted that in more complex cases where some fraction of the inlet fuel component remains unreacted, there is ambiguity in choosing the composition where the components cross the system boundary. In this paper, the fuel stream is assumed to have been fully converted either chemically or electrochemically, resulting in no such ambiguity.

2.3. Reversible FASOEC without oxygen evolution

One case that arises under the assumption that only electrochemical reactions occur in the anode is the possibility that oxygen gas is not produced, given the typically slow kinetics of the oxygen evolution reaction in comparison to the electrochemical oxidation rates of hydrogen, carbon monoxide, and methane. In this case, no oxygen gas exits

the anode, and the rate of reversible work crossing the system boundary for a steady molar flow rate of hydrogen is written as:

$$\dot{W}^{rev} = U_{H_2O}\dot{n}^{c,in}_{H_2O}\left(\Delta^*_r g_{H_2O} + \zeta_{H_2}\Delta^*_r g_{H_2}\right), \tag{30}$$

while the heat transfer rate is given by:

$$\dot{Q} = U_{H_2O}\dot{n}^{c,in}_{H_2O}\left(T\Delta^*_r s_{H_2O} + \zeta_{H_2}T\Delta^*_r s_{H_2}\right) - \dot{n}^{c,in}_{H_2O}\Delta_{in\text{-}out}h_{H_2O}, \tag{31}$$

where superscript * indicates that oxygen gas is not included in the evaluation of the changes in thermodynamic properties for a given oxidation reaction. Solving for the reversible potential in Eq. (30) yields:

$$E^{rev}_{H_2} = \frac{\Delta^*_r g_{H_2O} + \zeta_{H_2}\Delta^*_r g_{H_2}}{2F}, \tag{32}$$

where the Gibbs free energy required to facilitate the electrochemical reduction of steam in the cathode is expressed as:

$$\Delta^*_r g_{H_2O} = \Delta^*_r g^\circ_{H_2O}(T) + RT\ln\left(\frac{x^{c,out}_{H_2}}{x^{c,in}_{H_2O}}\right), \tag{33}$$

and the Gibbs free energy exploited in the electro-oxidation of hydrogen in the anode is written according to:

$$\Delta^*_r g_{H_2} = \Delta^*_r g^\circ_{H_2}(T) + RT\ln\left(\frac{x^{a,out}_{H_2O}}{x^{a,in}_{H_2}}\right). \tag{34}$$

For an arbitrary fuel mixture supplied to the anode, the reversible potential of an FASOEC is therefore expressed as follows:

$$E^{rev}_{mix,elec} = \frac{(z_{max}/2)\Delta^*_r g_{H_2O} + \zeta_{mix,elec}\sum_i (z_{max}/z_i)x^{a,in}_i\Delta^*_r g_i}{z_{max}F}, \tag{35}$$

and the ratio of the fuel mixture supplied to the anode to the amount of hydrogen produced that is required to perform electrolysis at a desired temperature and to supplement the entropy change of said reaction is denoted by:

$$\zeta_{mix,elec} = \frac{\Delta_{in\text{-}out}h_{H_2O} - U_{H_2O}T\Delta^*_r s_{H_2O}}{U_{H_2O}\sum_i x^{a,in}_i T\Delta^*_r s_i}. \tag{36}$$

2.4. Reversible FASOEC with combustion in anode

Having developed expressions for the performance of an FASOEC under the assumption that the supplied fuel reacts in a purely electrochemical manner, we now shift our focus to the opposite extreme, wherein fuel reacts chemically with the evolved oxygen in the anode. In this case, if hydrogen is supplied to the anode and reacts chemically, the $-\dot{n}^{a,in}_{H_2}\Delta_r h_{H_2}$ term in Eq. (5) is liberated as heat, and the Gibbs free energy change of hydrogen oxidation is not available to reduce the work input to conduct steam electrolysis. This presents a challenge in being able to control the operating temperature of a cell as a result of the chemical oxidation of fuel, and we therefore develop strategies to maintain its temperature at a fixed value. Accordingly, the rate of reversible work of the system is simplified to:

$$\dot{W}^{rev} = \dot{n}^{c,in}_{H_2O}U_{H_2O}\Delta_r g_{H_2O}. \tag{37}$$

with the reversible potential written as:

$$E^{rev}_{mix,comb} = \frac{\Delta_r g_{H_2O}}{2F}, \tag{38}$$

and the rate of heat transfer crossing the system boundary is modified from Eq. (7) to yield:

$$\dot{Q} = \dot{n}^{c,in}_{H_2O}U_{H_2O}\left(T\Delta_r s_{H_2O} + \zeta_{H_2}\Delta_r h_{H_2}\right) - \dot{n}^{c,in}_{H_2O}\Delta_{in-out}h_{H_2O}. \tag{39}$$

Eq. (39) is used to calculate the molar flow rate of fuel required to supply the thermal energy demands of the process such that the heat input is minimized (*i.e.* $\dot{Q} = 0$). The enthalpy change of the combustion of fuel provides the amount of thermal energy required for the entropy change of steam electrolysis, as well as the necessary sensible energy to compensate for the temperature difference between the inlet feed of steam and the system. The ratio of hydrogen supplied to the anode to the amount produced in the cathode is therefore expressed as:

$$\zeta_{H_2,comb} = \frac{\Delta_{in\text{-}out}h_{H_2O} - U_{H_2O}T\Delta_r s_{H_2O}}{U_{H_2O}\Delta_r h_{H_2}}, \tag{40}$$

and for an arbitrary fuel mixture supplied to the anode, this ratio is written according to:

$$\zeta_{mix,comb} = \frac{\Delta_{in\text{-}out}h_{H_2O} - U_{H_2O}T\Delta_r s_{H_2O}}{U_{H_2O}\sum_i x^{a,in}_i\Delta_r h_i}. \tag{41}$$

Again, this approach represents the opposite limiting case to pure electrochemical oxidation in the anode.

For cases when one component reacts electrochemically (denoted by subscript *lc* for limiting case) and the others react *via* combustion, the ratio of fuel supplied to the anode to the amount of hydrogen produced in the cathode is expressed as:

$$\zeta_{mix,lc} = \frac{\Delta_{in\text{-}out}h_{H_2O} - U_{H_2O}T\Delta_r s_{H_2O}}{U_{H_2O}\left(\sum_i x^{a,in}_i\Delta_r h_i + x^{a,in}_{lc}T\Delta_r s_{lc}\right)}. \tag{42}$$

In cases when hydrogen reacts electrochemically and the other fuels react chemically, for example, the above expression is written as:

$$\zeta_{mix,H_2} = \frac{\Delta_{in\text{-}out}h_{H_2O} - U_{H_2O}T\Delta_r s_{H_2O}}{U_{H_2O}\left(\sum_i x^{a,in}_i\Delta_r h_i + x^{a,in}_{H_2}T\Delta_r s_{H_2}\right)}, \tag{43}$$

and the reversible potential is evaluated using a similar expression to Eq. (13), except the changes in molar fraction of each component must be accounted for in the Gibbs free energy term, due to the changes in molar balances as a result of the fuel mixture, as shown in Appendix for FT tail gas.

2.5. FASOEC with irreversibilities

During the operation of an FASOEC, there will be instances when the supplied voltage is higher than the reversible potential, resulting in irreversibilities in the system. Accordingly, the entropy production term in Eq. (8) is expressed as:

$$\wp_s = \frac{I(V - E^{rev})}{T} = \frac{I^2R^e}{T} = \frac{i^2R_{ASR}}{T}A^e, \tag{44}$$

where V is the overpotential of the cell, R^e is the ionic resistance of the electrolyte, i is the current density, R_{ASR} is the area specific resistance of the electrolyte, and A^e is the in-plane area of the electrolyte. Upon substitution of Eq. (44) into Eq. (8), the rate of work crossing the system boundary is expressed as:

$$\dot{W} = IV = \dot{n}^{c,in}_{H_2O}U_{H_2O}\left(\Delta_r g_{H_2O} + \zeta_{H_2}\Delta_r g_{H_2}\right) + I^2R^e, \tag{45}$$

and the resultant heat transfer rate is denoted by:

$$\dot{Q} = \dot{n}^{c,in}_{H_2O}U_{H_2O}\left(T\Delta_r s_{H_2O} + \zeta_{H_2}T\Delta_r s_{H_2}\right) - \dot{n}^{c,in}_{H_2O}\Delta_{in-out}h_{H_2O} - I^2R^e. \tag{46}$$

Again, it is assumed that the sensible energy difference between the inlet and cell has been converted to heat without any work extraction. The ionic resistance of the electrolyte in an FASOEC can, to a reasonable approximation, be regarded as the only significant irreversible term in this process, and is given as:

$$R^e = \frac{\delta^e}{\sigma^e}\frac{1}{A^e}, \tag{47}$$

where δ^e is the electrolyte thickness and σ^e is the ionic conductivity. Often, however, a lumped area specific resistance (R_{ASR}) is measured for a given cell, such that:

$$R^e = \frac{R_{ASR}}{A^e}. \tag{48}$$

The area specific resistance used in this analysis is $R_{ASR} = 0.15\ \Omega\ cm^2$, which corresponds to the ionic conductivity of an 8% yttrium-doped

zirconium oxide electrolyte of thickness $\delta^e = 100$ μm at an operating temperature of 1123 K (850 °C) [56]. Ohmic heating I^2R^e is a key energy term in an SOEC for at least two reasons: it dictates the electrical energy input as well as the demand for other heat sources. The Ohmic heating of a cell depends on cell geometry (δ^e and A^e) and operating temperature, since the conductivity follows an Arrhenius temperature behaviour.

Accounting for Ohmic losses across the electrolyte, the cell potential of an FASOEC with hydrogen supplied to the anode is expressed as:

$$E_{\mathrm{H_2}}^{cell} = E_{\mathrm{H_2}}^{rev} + iR_{\mathrm{ASR}} = \frac{\Delta_r g_{\mathrm{H_2O}} + \zeta_{\mathrm{H_2}} \Delta_r g_{\mathrm{H_2}}}{2F} + iR_{\mathrm{ASR}}, \tag{49}$$

and the molar flow rate of hydrogen supplied to the anode relative to the amount produced in the cathode is denoted by:

$$\zeta_{\mathrm{H_2}} = \frac{\Delta_{in\text{-}out} h_{\mathrm{H_2O}} + 2FU_{\mathrm{H_2O}} iR_{\mathrm{ASR}} - U_{\mathrm{H_2O}} T\Delta_r s_{\mathrm{H_2O}}}{U_{\mathrm{H_2O}} T\Delta_r s_{\mathrm{H_2}}}, \tag{50}$$

which can be modified to account for a mixture of fuels that react *via* electrochemical and chemical reaction pathways.

3. Results and discussion

Since the FT tail gas produced in the PBtL process can be redirected from the entrained flow gasifier to the anode of an SOEC, we are interested in how much the operating potential (or equivalently the input power) can be reduced for a given flow rate of fuel. Additionally, we are also interested in addressing the following questions: How much fuel is required to minimize the oxygen partial pressures in the anode, as well as to heat the inlet flow of steam to the operating temperature of a cell? How do irreversibilities in the system (*i.e.* Ohmic overpotential and heating) affect these amounts? How does the reaction pathway of the fuel influence the operating potential of an FASOEC?

Another aspect that we account for in this analysis is the use of staged electrolysis. This is important when utilizing an external heat source, such as the residual heat from an entrained flow gasifier in the PBtL process, because the reversible heat demands of the electrolysis reaction change when fuel is introduced to the anode of an SOEC. Furthermore, meeting the reversible heat demands often requires that steam is supplied to a cell at temperatures hundreds of degrees above the operating temperature, unless the electrolysis process is conducted in stages. Herein, we consider two stages of electrolysis in series with a steam utilization factor of $U_{\mathrm{H_2O}} = 0.4$, where half the amount of steam is converted at each stage, resulting in a final utilization of $U_{\mathrm{H_2O}} = 0.8$. These results are compared with those obtained in single-stage electrolysis, with a utilization factor of $U_{\mathrm{H_2O}} = 0.8$. The questions and concerns posed above are addressed in the following sections.

3.1. Electrical work input reduction in FASOECs

In order to quantify the electrical work input reduction of steam electrolysis as a result of supplying fuel to the anode of an SOEC, we must first examine the effects of the ratio of fuel delivered to hydrogen produced. Fig. 5(a) illustrates both standard and reversible potentials of an FASOEC fed with pure hydrogen, carbon monoxide, and methane, as functions of the ratio of fuel supplied to hydrogen generated, ζ_i, for a steam utilization factor of $U_{\mathrm{H_2O}} = 0.4$. The reversible potential differs from the standard potential, given that the former considers the variations in component molar fractions as a result of the changes in ζ_i, while the latter assumes unity for each component. For all cases when $\zeta_i < 1$, it is shown that the magnitude of the operating potential required to perform electrolysis decreases as increasing molar flow rates of fuel relative to hydrogen produced are supplied to the anode, with CH_4-assisted and CO-assisted yielding the highest and lowest reductions, respectively. This result corresponds to the fact that a higher portion of the Gibbs free energy associated with the fuel is exploited as ζ_i increases, causing a net decrease in the electrical work input. It is also shown that the reversible potentials are closer to zero in comparison to the standard potentials, since the molar fraction of oxygen is lower as a result of the oxide ions reacting with the supplied fuel, as demonstrated in Fig. 5(a). Furthermore, both standard and reversible potentials for H_2- and CO-assisted electrolysis are nearly identical, since the Gibbs free energy released by both fuels are virtually the same and their respective molar balances in the anode are analogous to one another, according to Eqs. (16) and (20). These expressions indicate that the oxygen molar fraction is equal to zero when the supplied fuel is at parity with the amount of hydrogen produced in the cathode (*i.e.* $\zeta_{\mathrm{H_2}}$ and $\zeta_{\mathrm{CO}} = 1$). For CH_4-assisted electrolysis, however, the oxygen molar fraction is equal to zero when methane is supplied at one-quarter the rate at which hydrogen is produced, according to Eq. (24), since methane consumes four-times the number of oxide ions in comparison to H_2- and CO-assisted electrolysis. This causes the reversible potential of CH_4-assisted electrolysis to approach an asymptote at $\zeta_{\mathrm{CH_4}} = 0.25$, at which point the reversible potential coincides with the value corresponding to standard conditions with $\zeta_{\mathrm{CH_4}} = 1$. This reduction in operating potential has also been observed in previous experiments [42,57], wherein the difference in operating potentials between an SOEC and a CH_4-assisted SOEC was reported to be approximately 1 V. A reversible potential equal to 0 V indicates that the energy exploited by the addition of fuel in the anode is equal to that required to perform steam electrolysis. It is important to note that CH_4-assisted electrolysis on a molar basis requires only one quarter the amount of fuel to drive the oxygen molar fraction to zero in comparison to H_2- and CO-assisted electrolysis. This illuminates an advantage of supplying a methane-rich fuel mixture to the anode of an SOEC, which corresponds to the tail gas of an FT reactor in the PBtL process. We consider the ratio of the inlet molar flow rate of fuel to the molar production rate of hydrogen as an input parameter in this analysis, since it enables designers to conveniently predict the reductions in electrical work input of an FASOEC based on the amount of tail gas produced and the amount of hydrogen required by the entire processing plant. When the rate at which fuel is supplied exceeds the rate of hydrogen production (*i.e.* $\zeta_i > 1$), the standard potentials become independent of ζ_i, because the supplied fuel behaves as both a sweep gas and fuel due to the limited number of oxide ions available to react electrochemically in the anode. Similar results are demonstrated in Fig. 5(b) for the reversible potentials, except a higher electrical work input is required to facilitate steam electrolysis, since the utilization factor of steam is increased to $U_{\mathrm{H_2O}} = 0.8$.

Having established the effects of the ratio of the inlet molar flow rate of fuel to the molar production rate of hydrogen on the operating potential of an FASOEC for individual fuel components, we now shift our attention to a fuel mixture comprising of hydrogen (57%), carbon monoxide (28%), and methane (14%). Fig. 5(c) and (d) illustrates the standard, reversible, and cell potentials (*i.e.* including Ohmic overpotential) versus the ratio of fuel supplied to hydrogen produced, with steam utilization factors of $U_{\mathrm{H_2O}} = 0.4$ and 0.8, respectively. The standard potential of the fuel mixture produces similar results to those observed for individual fuel components in Fig. 5(a) and (b), with its operating potential located between those of pure CH_4- and H_2-assisted electrolysis. Additionally, the reversible potential approaches an asymptote when $\zeta_{mix,elec} = 0.704$, which corresponds to the ratio of fuel supplied to hydrogen produced which drives the oxygen molar fraction to zero (see Appendix for derivation). At the threshold value of $\zeta_{mix,elec}$, the reversible potential coincides with that of the standard potential, which is labelled as the fuel mixture supply limit potential in Fig. 5(c) and (d). This threshold value is a crucial operating parameter, since it represents the limit beyond which no oxygen is present in the anode, resulting in significant efficiency improvements for the FASOEC and consequently the PBtL process.

When evaluating the reductions in electrical work input required to perform steam electrolysis, it is also important to account for the effects of irreversibilities in the system. In this analysis, we consider the Ohmic overpotential across the electrolyte to be the main contributor

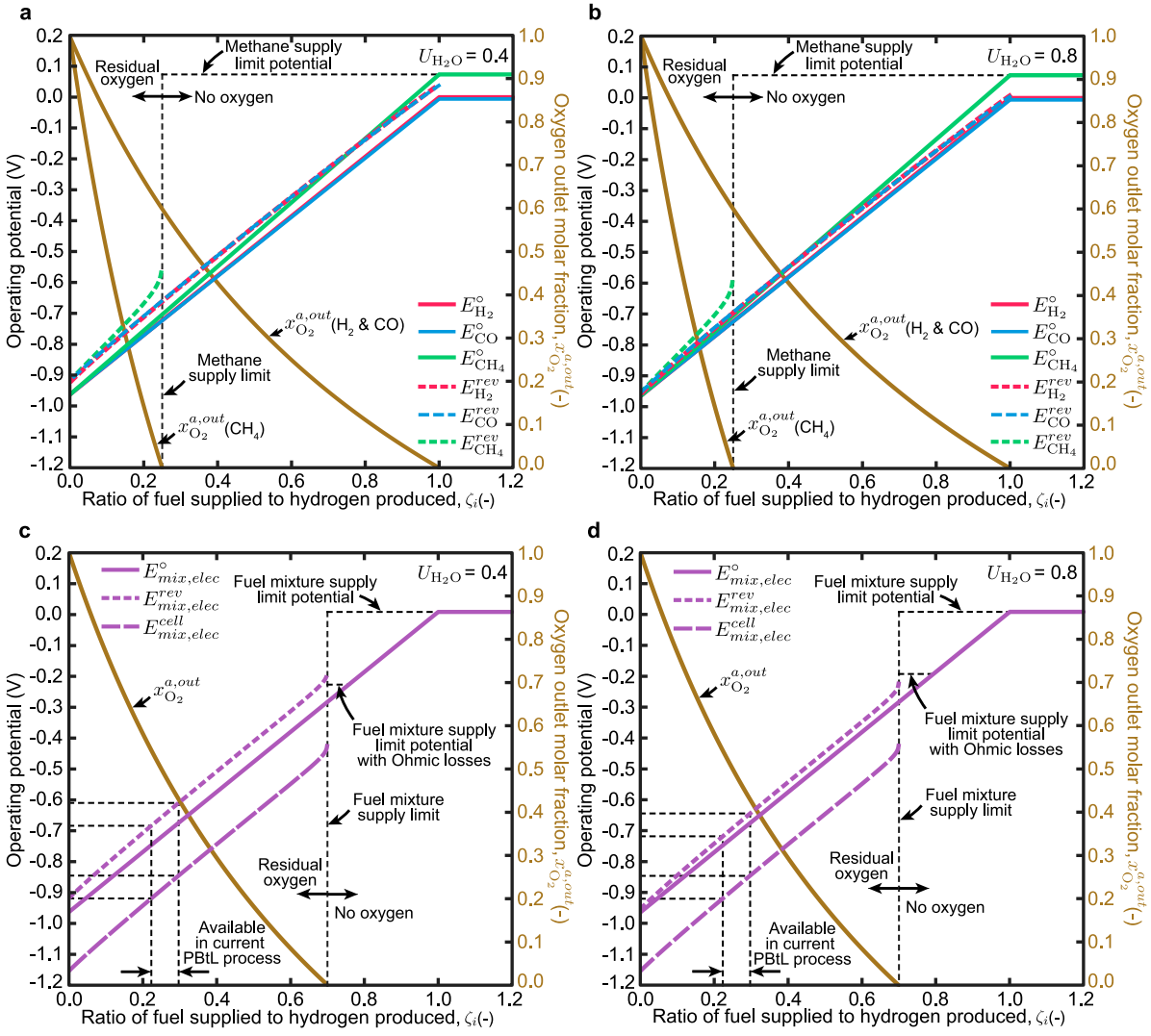

Fig. 5. Operating potentials (leftmost vertical axes) and oxygen outlet molar fraction (rightmost vertical axes), $x_{O_2}^{a,out}$, as functions of the ratio of fuel supplied to hydrogen produced, ζ_i, for: (a–b) pure H_2-, CO-, and CH_4-assisted electrolysis, with (a) $U_{H_2O} = 0.4$ and (b) $U_{H_2O} = 0.8$; (c–d) FT tail gas-assisted electrolysis, with (c) $U_{H_2O} = 0.4$ and $i = 1.57$ A cm^{-2}, and (d) $U_{H_2O} = 0.8$ and $i = 1.34$ A cm^{-2}. Range of ζ_i values available in current PBtL process is labelled in (c) and (d).

to irreversibilities, using the ionic conductivity of an 8% yttrium-doped zirconium oxide, which has a value of $\sigma^e = 6.67 \times 10^{-4}$ S cm^{-1} at a temperature of 1123 K (850 °C) [56], and an electrolyte thickness of $\delta^e = 100$ μm, for an area specific resistance of $R_{ASR} = 0.15$ Ω cm^2. Current densities of $i = 1.57$ A cm^{-2} and 1.34 A cm^{-2} for steam utilization factors of $U_{H_2O} = 0.4$ and 0.8, respectively, were selected to compute the Ohmic overpotentials, as these values correspond to the threshold value of $\zeta_{mix,elec}$ that matches the heating demands of a cell when its operating temperature is equal to the steam inlet temperature when all fuel components react electrochemically (see discussion in next sub-section). These current densities produce Ohmic overpotentials of 0.24 V and 0.21 V in Fig. 5(c) and (d), respectively, which consequently increase the magnitude of the operating potential required to generate hydrogen. Without Ohmic overpotentials, using the tail gas from an FT reactor lowers the electrical work input by approximately 75% for conditions when oxygen is produced in the anode (*i.e.* $\zeta_{mix,elec} < 0.704$), which we refer to as the sub-limiting case. For conditions when $\zeta_{mix,elec} \geq 0.704$ and thus no oxygen is produced (*i.e.* super-limiting case), the electrical work input is reduced to nearly zero. Including Ohmic overpotentials results in approximately 60% and 80% reductions in the electrical work input for sub-limiting and super-limiting cases, respectively, with negligible differences between steam utilization factors of $U_{H_2O} = 0.4$ and 0.8, as shown in Fig. 5. It is also shown in Fig. 5(c) and (d) that the ratio of fuel supplied to hydrogen produced available in the current PBtL process (*i.e.* $\zeta_{mix,elec} \approx 0.26$) results in reductions in the electrical work input by approximately 23% with the inclusion of the Ohmic overpotential. The cases illustrated in Fig. 5(c) and (d) account for the balance between Ohmic heating and the entropy change required to perform electrolysis, while Fig. 5(a) and (b) presents cases wherein only the minimum electrical work input is considered. In reality, there may be a need to supply a sufficient amount of thermal energy in order to heat an inlet supply of steam to the operating temperature of a given cell, therefore making it more conducive to performing electrolysis in stages, in addition to satisfying the entropic heat demands of the electrolysis reaction. The rate at which fuel needs to be supplied to a cell to meet these heating demands for the five limiting cases is revealed below.

3.2. Heating demands of FASOECs

When introducing a multi-component fuel mixture to the anode of an SOEC, it is possible there will be competing effects between the chemical and electrochemical oxidation of fuel, due to the production of oxygen in the anode and the ability of the fuel to diffuse/convect towards the catalyst surface. Insufficient amounts of fuel will likely result in the former reaction pathway, thus liberating the entire reaction

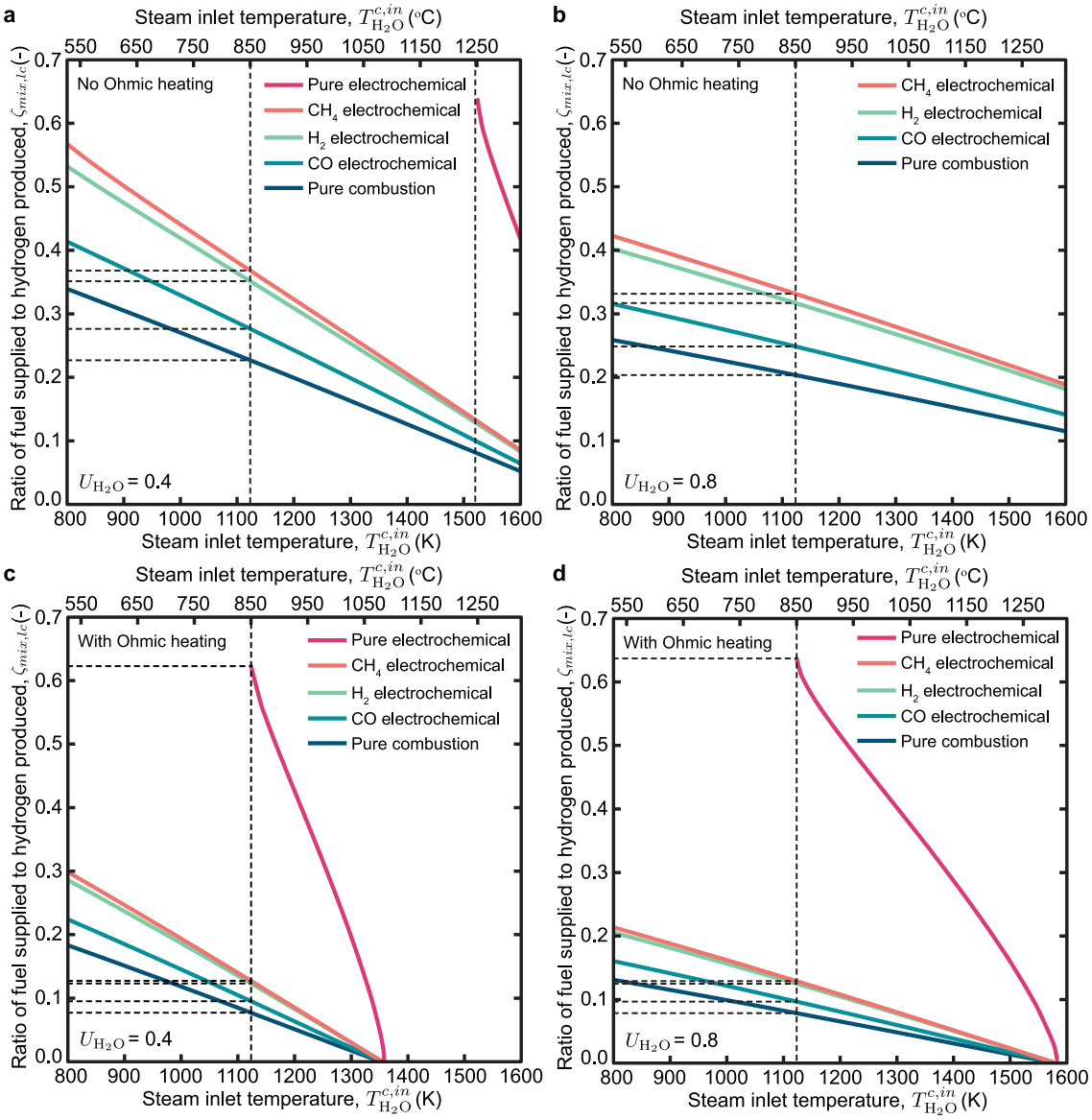

Fig. 6. Ratio of fuel supplied to hydrogen produced, ζ_i, required to heat inlet flow of steam to cell operating temperature (T = 1123 K) as a function of steam inlet temperature, $T^{c,in}_{H_2O}$, for (a–b) no Ohmic heating with (a) U_{H_2O} = 0.4 and (b) U_{H_2O} = 0.8; and (c–d) with Ohmic heating for (c) U_{H_2O} = 0.4 and i = 1.57 A cm^{-2} and (d) U_{H_2O} = 0.8 and i = 1.34 A cm^{-2}. Limiting cases are displayed in each sub-figure.

enthalpy in the form of heat, while supplying increased amounts of fuel beyond the super-limiting case (*i.e.* $\zeta_{mix,elec} \geq 0.704$) will cause the oxygen molar fraction to equal zero, therefore resulting in the electrochemical oxidation of fuel. This would lead to significant reductions in the electrical work input, and only the entropic component of the oxidation reaction is available to the cell as heat. As mentioned above, a detailed kinetic analysis to determine the relative proportion of chemical and electrochemical reactions is beyond the scope of this study, and we therefore investigate five limiting cases: (*i*) all components react *via* combustion, (*ii*) hydrogen reacts electrochemically with the remaining components reacting *via* combustion, (*iii*) carbon monoxide reacts electrochemically with the remaining components reacting *via* combustion, (*iv*) methane reacts electrochemically with the remaining components reacting *via* combustion, and (*v*) all components react electrochemically. Additionally, we consider different steam utilization factors of U_{H_2O} = 0.4 and 0.8: the former representing electrolysis performed in two stages and the latter corresponding to single-stage electrolysis.

Fig. 6 demonstrates the ratio of the inlet molar flow rate of the fuel mixture to the molar production rate of hydrogen required to provide the thermal energy demands to maintain a cell operating temperature of 1123 K (850 °C), as a function of the inlet temperature of steam for each of the limiting cases considered. Irrespective of the utilization factor of steam and whether Ohmic heating occurs in the system, it is shown that the chemical reaction pathway of each component requires the lowest flow rate of fuel to satisfy the heating demands of the cell, whereas the pure electrochemical reaction pathway requires the highest amount. Additionally, for the electrochemical reaction pathway of individual fuel components, it is revealed that carbon monoxide oxidation requires the lowest flow rate of fuel, with methane oxidation needing the highest.

For a steam utilization factor of U_{H_2O} = 0.4 and no Ohmic heating, it is shown in Fig. 6(a) that the entropic heat produced *via* pure electrochemical oxidation is insufficient to match the heating demands of a cell that operates at a temperature of 1123 K (850 °C), with an inlet flow of steam supplied at the same temperature. This limitation is imposed by the threshold value of $\zeta_{mix,elec}$ = 0.704, where ratios of fuel supplied to hydrogen produced greater than or equal to this value causes the oxygen molar fraction to equal zero. Without Ohmic

heat generation, meeting the heat demands of a cell requires that steam is supplied at temperatures exceeding approximately 1520 K (1247 °C), which can be attained by superheating the steam with the thermal energy provided by the entrained flow gasifier in the PBtL process. Furthermore, the heat offered by the supplied fuel can be replaced entirely by that provided by the inlet flow of steam with a temperature of approximately 1750 K (1477 °C) for each limiting case, as shown in Fig. 6(a). However, supplying the inlet flow of steam at such temperatures would impose several design challenges, including the management of thermal gradients within a cell, thus illuminating the advantages of delivering fuel to the anode of an SOEC to serve as a heat source. If the ratio of fuel supplied to hydrogen produced is higher than that corresponding to the dashed, horizontal lines shown in Fig. 6(a) for a steam inlet temperature of 1123 K (850 °C), the operating temperature of the cell would consequently increase, whereas lower values of ζ_i would cause the cell to cool. It is therefore critical that the flow rate of fuel is chosen carefully in order to meet the heating demands of a cell and to limit the risk of elevated thermal stresses within the assembly of a cell. These results are largely similar to those found for a steam utilization factor of $U_{H_2O} = 0.8$, except lower flow rates of fuel are required when the utilization factor of steam is increased, as illustrated in Fig. 6(b), and the inlet temperature of steam at which no fuel is required to heat the cell is approximately 2250 K (1977 °C).

In addition to the inlet molar flow rate of fuel and steam delivered to an FASOEC, Ohmic heat generation caused by the transport of oxide ions through the electrolyte can be leveraged to supplement the head demands of a cell. Fig. 6(c) and (d) illustrate the additional effects of Ohmic heating on the ratio of fuel supplied to hydrogen produced that is required to meet the heating demands of a cell, as a function of the inlet temperature of steam, with steam utilization factors of $U_{H_2O} = 0.4$ and 0.8, respectively. The same current densities and electrolyte specifications described above are implemented here for the corresponding steam utilization factors (*i.e.* $U_{H_2O} = 0.4$ with $i = 1.57$ A cm^{-2} and $U_{H_2O} = 0.4$ with $i = 1.57$ A cm^{-2}). These current densities were selected since they yield nearly the same $\zeta_{mix,elec}$ value as the threshold value of 0.704 that meets the heating demands of a cell when its operating temperature is equal to the inlet temperature of steam (*i.e.* $\zeta_{mix,elec} = 0.623$ and 0.637 for $U_{H_2O} = 0.4$ and 0.8, respectively). The exact value of 0.704 could not be attained because the oxygen molar fraction is equal to zero at this value, resulting in a divergent solution when performing iterations. It is shown in Fig. 6(c) and (d) that Ohmic heating lowers the amount of fuel required to maintain a cell operating temperature of 1123 K (850 °C). Consequently, the inlet temperature of steam at which no fuel is needed to heat the cell is also lowered from 1750 K (1477 °C) to 1360 K (1087 °C) and 2250 K (1977 °C) to 1580 K (1307 °C) for steam utilization factors of $U_{H_2O} = 0.4$ and 0.8, respectively. Again, it should be noted that supplying steam to the cathode at such temperatures would cause serious damage to a cell, and demonstrates the benefits of supplying fuel to the anode of an SOEC to meet its heating requirements. Increasing the current density therefore reduces the ratio of fuel supplied to hydrogen produced and the inlet temperature of steam needed to satisfy heating requirements. This approach enables designers and researchers to select appropriate specifications for the electrolyte (*i.e.* conductivity and thickness), as well as values of the operating parameters of a cell, in order to match the thermal energy demands for a given reaction pathway.

3.3. Heat and work requirements of FASOECs

Now that we have determined the ratios of fuel supplied to hydrogen produced that are necessary to meet the thermal energy demands of an FASOEC in order to operate at a constant temperature, we reveal how these values affect the electrical work input. Fig. 7 illustrates the resultant operating potentials and corresponding ratios of fuel supplied to hydrogen produced (also shown in Fig. 6) versus the inlet temperature of steam. Fig. 7(a) and (b) demonstrate these results without Ohmic overpotentials and heating, with steam utilization factors of $U_{H_2O} = 0.4$ and 0.8, respectively, while Fig. 7(c) and (d) account for these irreversibilities. It is shown in each sub-figure that the standard potential for steam electrolysis, $E^{\circ}_{H_2O}$, maintains a constant value of −0.963 V at an operating temperature of 1123 K (850 °C), since this potential corresponds to no fuel assistance (*i.e.* $\zeta_{mix,lc} = 0$) and the molar fraction of each component is unity. It should be noted that the increases in electrical work input for standard conditions are a result of the Ohmic overpotential, as shown in Fig. 7(c) and (d) (*i.e.* 0.24 V for $U_{H_2O} = 0.4$ and 0.21 V for $U_{H_2O} = 0.8$). The standard potential of steam electrolysis is illustrated to serve as a reference in order to demonstrate the electrical work input reductions for the five limiting cases of fuel-assisted electrolysis.

As mentioned above, the chemical reaction pathway of each fuel component requires the lowest ratio of fuel supplied to hydrogen produced to satisfy the heating demands of an FASOEC, whereas pure electrochemical oxidation requires the highest ratio, as shown in Figs. 6 and 7. Consequently, it is demonstrated in Fig. 7 that the pure electrochemical reaction pathway of the supplied fuel results in the highest reductions in the electrical work input, while the combustion of each fuel component experiences the lowest reductions. This is because increasing the ratio of the flow rate of fuel supplied to hydrogen produced enables a higher portion of the Gibbs free energy of the electrochemical oxidation of fuel to be exploited, thus yielding greater reductions in the electrical work input. The variations in the operating potential for the case of pure combustion is a result of the changes in the oxygen molar fraction, since the operating potential of this case is otherwise independent of $\zeta_{mix,comb}$, according to Eq. (38).

Another important aspect to consider is the proportion with which each fuel component is delivered to a cell. For the electrochemical oxidation of an individual fuel component, we previously revealed that carbon monoxide requires the lowest ratio of fuel supplied to hydrogen produced, with methane requiring the highest values. In this analysis, hydrogen, carbon monoxide, and methane are delivered to the anode with inlet molar fractions of 0.57, 0.29, and 0.14, respectively, which results in nearly proportional reductions in the electrical work input when considering the electrochemical reaction pathway of an individual fuel component, as shown in Fig. 7. For all cases examined in this analysis, increasing the steam inlet temperature results in increases in the electrical work input, since the heating demands from the fuel are mitigated, thus yielding lower values of $\zeta_{mix,lc}$. The reductions in electrical work input when the operating temperature of the cell is equal to that of the inlet steam (*i.e.* $T = 1123$ K) are summarized in Table 1, alongside the corresponding ratios of fuel supplied to hydrogen produced for steam utilization factors of $U_{H_2O} = 0.4$ and 0.8. As a result of this analysis, designers can determine how much fuel is required to match the heating demands of an FASOEC and predict the consequent electrical work input reductions for a particular reaction pathway of the supplied fuel. Given the typically slow kinetics of the oxygen evolution reaction in comparison to those of the electrochemical oxidation of hydrogen, carbon monoxide, and methane, it is expected that the latter will dominate the combustion reaction pathway. This hypothesis is supported by the similarities between the results corresponding to the pure electrochemical reaction pathway and those observed in previous experiments (*i.e.* 50% reduction in electrical work input from Pham et al. [41]), but requires a detailed kinetic analysis in order to ascertain the main reaction pathways.

3.4. Contribution to the PBtL process

A broader objective of the current study is to examine how redirecting the tail gas of an FT reactor to the anode of an SOEC lowers the electricity demand of the PBtL process, assuming the same amount of input biomass and producing an equal amount of fuel as found in

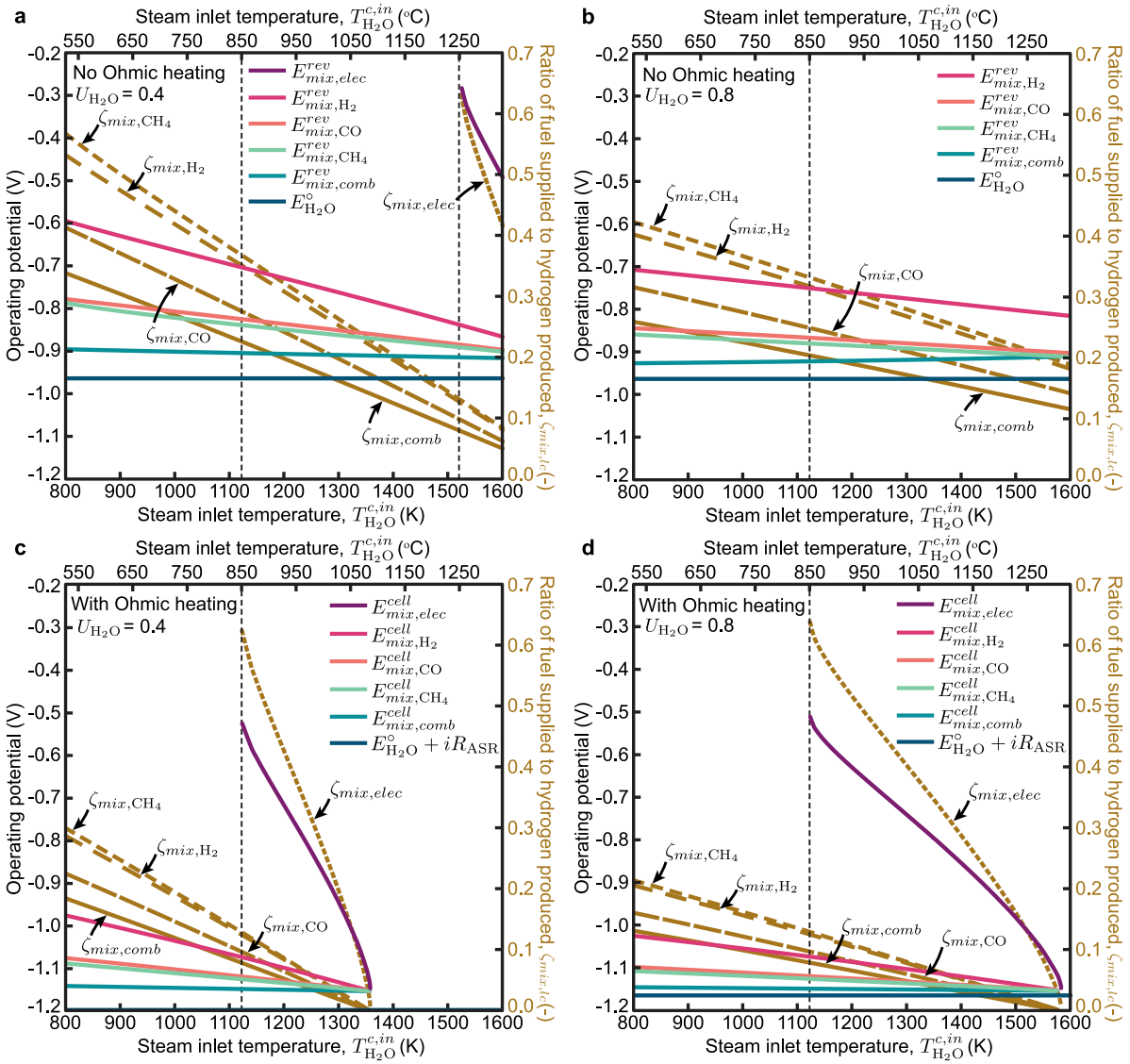

Fig. 7. Resultant operating potentials (leftmost vertical axes) and corresponding ratios of fuel supplied to hydrogen produced (rightmost vertical axes), ζ_i, required to heat inlet flow of steam to cell operating temperature (850 °C) as functions of the steam inlet temperature, $T^{c,in}_{H_2O}$, for (a–b) no Ohmic heating with (a) $U_{H_2O} = 0.4$ and (b) $U_{H_2O} = 0.8$; and (c–d) with Ohmic heating for (c) $U_{H_2O} = 0.4$ and $i = 1.57$ A cm^{-2} and (d) $U_{H_2O} = 0.8$ and $i = 1.34$ A cm^{-2}.

Table 1
Summary of operating potentials and corresponding ratios of fuel supplied to hydrogen produced required to heat FASOEC, when $T^{c,in}_{H_2O} = T = 1123$ K for steam utilization factors of $U_{H_2O} = 0.4$ and 0.8, as shown in Fig. 7.

Limiting case	$U_{H_2O} = 0.4$				$U_{H_2O} = 0.8$			
i (A cm^{-2})	0		1.57		0		1.34	
Parameter:	$E^{rev}_{mix,lc}$ (V)	ζ_i (–)	$E^{cell}_{mix,lc}$ (V)	ζ_i (–)	$E^{rev}_{mix,lc}$ (V)	ζ_i (–)	$E^{cell}_{mix,lc}$ (V)	ζ_i (–)
No fuel assistance	−0.963	0	−1.199	0	−0.963	0	−1.164	0
Pure combustion	−0.904	0.226	−1.149	0.078	−0.922	0.204	−1.148	0.079
H_2 electrochemical	−0.703	0.351	−1.075	0.124	−0.750	0.318	−1.073	0.125
CO electrochemical	−0.824	0.275	−1.120	0.096	−0.867	0.249	−1.119	0.097
CH_4 electrochemical	−0.834	0.367	−1.126	0.128	−0.880	0.332	−1.125	0.129
Pure electrochemical ($x^{a,out}_{O_2} > 0$)	N/A	N/A	−0.526	≤0.623	N/A	N/A	−0.511	≤0.637
Pure electrochemical ($x^{a,out}_{O_2} = 0$)	N/A	N/A	−0.240	≥0.704	N/A	N/A	−0.210	≥0.704

the study conducted by Hillestad et al. [34], who developed an in-depth model of the PBtL process (all process details are found in this article). We also assume that the external carbon flow remains constant and the electrical power demand of the entire PBtL process is directly proportional to the operating potential of an FASOEC. Preliminary comparisons of the electrical energy inputs and energy efficiencies between the BtL, PBtL, and FAPBtL processes are shown in Table 2. Additionally, for the FAPBtL process in particular, we compare these metrics for the $\zeta_{mix,elec}$ value available in the current PBtL process, which corresponds to a value of approximately $\zeta_{mix,elec} = 0.260$, as well as for the sub-limiting case (*i.e.* $x^{a,out}_{O_2} > 0$ with $\zeta_{mix,elec} = 0.637$) when the cell operating temperature and steam inlet temperature are both equal

Table 2
Comparison of the electrical energy input requirements and energy efficiencies between the BtL, PBtL, and FAPBtL processes, with ratios of fuel supplied to hydrogen produced available in current PBtL process ($\zeta_{mix,elec} = 0.260$) and for sub-limiting case ($\zeta_{mix,elec} = 0.637$).

Process type	Inlet units			Outlet units		Efficiency (%)	
	Carbon	Biomass energy	Electrical energy	Carbon	Fuel energy	Carbon	Energy
BtL	100	100	0	38	53	38	53
PBtL	100	100	95	91	128	91	66
FAPBtL ($\zeta_{mix,elec} = 0.260$)	100	100	72	91	128	91	74
FAPBtL ($\zeta_{mix,elec} = 0.637$)	100	100	42	91	128	91	90

to 1123 K (850 °C). Each of these cases assume pure electro-oxidation of the supplied fuel and a steam utilization factor of $U_{H_2O} = 0.8$. For the FAPBtL process with $\zeta_{mix,elec} = 0.260$, it is shown that the electrical energy input can be decreased from 95 units (−1.164 V) to 72 units (−0.882 V, see Fig. 5(d)), resulting in an improvement in system energy efficiency of 65% to 74%. If the ratio of the supplied fuel to hydrogen produced could increase to approximately the threshold value of the sub-limiting case (*i.e.* $\zeta_{mix,elec} = 0.637$), the system efficiency would increase to 90% as a result of the electrical energy input decreasing to 42 units (−0.511 V, see Table 1). It is important to note that selecting an appropriate value of $\zeta_{mix,elec}$ requires consideration beyond simply decreasing the electrical work input of an SOEC; it also depends on the rate at which hydrogen must be supplied to the RWGS reactor in the PBtL process to yield a desired set of products, as well as the rate at which tail gas is produced by the FT reactor, which can result in relatively low values of $\zeta_{mix,elec}$ [34]. In other words, it may not be feasible to attain values of $\zeta_{mix,elec}$ that are close to its threshold value, and to therefore increase the energy efficiency of fuel production to 90%. It should be noted that these are simply preliminary calculations to assess the potential benefits of implementing an FASOEC in the PBtL process, and that determining the actual efficiency gains of the system requires a detailed process model, coupled with iterative techniques, to establish optimal operating conditions and FT tail gas compositions to augment FASOEC and FT performance. Nevertheless, this analysis illustrates the advantages of delivering the tail gas of an FT reactor to the anode of an SOEC in order to reduce the electrical work input required to generate hydrogen and to meet the heating demands of a cell.

4. Conclusions

In this study, a thermodynamic framework was developed to investigate the performance limits of fuel-assisted solid oxide electrolysis cells (FASOECs). By feeding the tail gas of a Fischer–Tropsch (FT) reactor in the power- and biomass-to-liquid fuel (PBtL) process to the anode of an SOEC, we demonstrated the amount by which the electrical work input required to facilitate steam electrolysis can be reduced for a given ratio of fuel supplied to hydrogen produced in a cell. We also revealed strategies to minimize oxygen partial pressures in the anode and elucidated how a particular reaction pathway of the supplied fuel (either chemical or electrochemical) influences the operating potential of an FASOEC. Furthermore, we determined the molar flow rates of fuel required to satisfy the heating demands of an FASOEC for a wide range of steam inlet temperatures delivered to the cathode. Finally, preliminary calculations were performed to evaluate potential improvements to the energy efficiency of the PBtL process as a result of redirecting the tail gas of an FT reactor to the anode of an SOEC, where it was estimated that efficiencies as high as 90% can be attained. Future work for this concept requires rigorous process modelling in order to obtain accurate predictions of the energy efficiency of fuel production by implementing an FASOEC in the PBtL process, and the eventual deployment of this technology necessitates further investigation, development, and experimental validation before it can be realized. Because of this analysis, designers will be able to select an appropriate ratio of fuel supplied to hydrogen produced in order to minimize oxygen partial pressures, match the heating requirements for a given steam inlet temperature, and reduce the electrical work input of an FASOEC to improve the efficiency of the PBtL process.

Obituary

The authors dedicate this paper to the late Dr. Jon G. Pharoah, who passed away November 19th, 2021, after a battle with cancer. Dr. Pharoah played a pivotal role in the development of this manuscript. He participated in discussions until the end of his life, and expressed a desire for this work to be published, for he believed it could contribute to the advancement of bio-based liquid fuels and help mitigate climate change. Over the course of his research career, Dr. Pharoah published more than 40 research articles on the computational modelling of transport phenomena in electrochemical energy systems, including solid oxide and polymer electrolyte membrane cells. He was continuously engaged in the research of his colleagues and students, and has made a lasting impact on those he encountered within the research community and beyond. He will be missed dearly.

CRediT authorship contribution statement

Anders S. Nielsen: Conceptualization, Methodology, Formal analysis, Visualization, Writing – original draft, Writing – review & editing. **M. Ostadi:** Conceptualization, Methodology, Writing – review & editing. **Bjørn Austbø:** Methodology, Writing – review & editing. **M. Hillestad:** Methodology, Writing – review & editing. **Gonzalo del Alamo:** Writing – review & editing. **Odne Burheim:** Conceptualization, Methodology, Formal analysis, Visualization, Writing – original draft, Writing – review & editing, Supervision.

Declaration of competing interest

The authors declare that they have no known competing financial interests or personal relationships that could have appeared to influence the work reported in this paper.

Acknowledgements

The Research Council of Norway (project no. 267989) is greatly acknowledged for the financial aid of this project. ENERSENSE, Norway and NTNU, Norway (project no. 68024013) is greatly acknowledged for the financial aid of this project. A.S. Nielsen gratefully acknowledges the funding support from a Natural Sciences and Engineering Research Council of Canada (NSERC) Postgraduate Scholarship (PGS-D3).

Appendix. Threshold value of ζ_{mix}

The threshold value of $\zeta_{mix} = \dot{n}^{a,in}_{mix}/U_{H_2O}\dot{n}^{c,in}_{H_2O}$ for a fuel mixture supplied to the anode stems from the molar balance of oxygen in the anode, which, in this case, is expressed as:

$$\dot{n}^{a,out}_{O_2} = \frac{1}{2}U_{H_2O}\dot{n}^{c,in}_{H_2O} - \frac{1}{2}\dot{n}^{a,in}_{H_2} - \frac{1}{2}\dot{n}^{a,in}_{CO} - 2\dot{n}^{a,in}_{CH_4}, \tag{A.1}$$

and the outlet molar flow rates of steam and carbon dioxide are denoted by: $\dot{n}^{a,out}_{H_2O} = \dot{n}^{a,in}_{H_2} + 2\dot{n}^{a,in}_{CH_4}$; and $\dot{n}^{a,out}_{CO_2} = \dot{n}^{a,in}_{CO} + \dot{n}^{a,in}_{CH_4}$, respectively, resulting in a total outlet molar flow rate of:

$$\dot{n}^{a,out}_{tot} = \frac{1}{2}U_{H_2O}\dot{n}^{c,in}_{H_2O} + \frac{1}{2}\dot{n}^{a,in}_{H_2} + \frac{1}{2}\dot{n}^{a,in}_{CO} + \dot{n}^{a,in}_{CH_4}. \tag{A.2}$$

The outlet molar fraction of oxygen is therefore given by:

$$x_{O_2}^{a,out} = \frac{\dot{n}_{O_2}^{a,out}}{\dot{n}_{tot}^{a,out}} = \frac{1 - \zeta_{mix}\left(x_{H_2}^{a,in} + x_{CO}^{a,in} + 4x_{CH_4}^{a,in}\right)}{1 + \zeta_{mix}\left(x_{H_2}^{a,in} + x_{CO}^{a,in} + 2x_{CH_4}^{a,in}\right)}, \quad (A.3)$$

where $x_i^{a,in} = \dot{n}_i^{a,in}/\dot{n}_{mix}^{a,in}$, and solving for ζ_{mix} when $x_{O_2}^{a,out} = 0$ yields:

$$\zeta_{mix} = \frac{1}{x_{H_2}^{a,in} + x_{CO}^{a,in} + 4x_{CH_4}^{a,in}}. \quad (A.4)$$

With inlet molar fractions 0.57, 0.29, and 0.14 for hydrogen, carbon monoxide, and methane, respectively, the threshold value is therefore $\zeta_{mix} = 0.704$. This approach was also used for pure hydrogen-, carbon monoxide-, and methane-assisted electrolysis, and can be applied to any fuel mixture delivered to the anode in order to determine the threshold at which the oxygen molar fraction is equal to zero.

References

[1] Hoegh-Guldberg O, Jacob D, Bindi M, Brown S, Camilloni I, Diedhiou A, et al. Impacts of 1.5 °C global warming on natural and human systems. Global warming of 1.5 °C. An IPCC special report, IPCC Secretariat; 2018.

[2] Goh BHH, Chong CT, Ong HC, Seljak T, Katrašnik T, Józsa V, Ng J-H, Tian B, Karmarkar S, Ashokkumar V. Recent advancements in catalytic conversion pathways for synthetic jet fuel produced from bioresources. Energy Convers Manage 2022;251:114974. http://dx.doi.org/10.1016/j.enconman.2021.114974.

[3] Fivga A, Speranza LG, Branco CM, Ouadi M, Hornung A. A review on the current state of the art for the production of advanced liquid biofuels. AIMS Energy 2019;7(1):46–76. http://dx.doi.org/10.3934/energy.2019.1.46.

[4] Korberg AD, Mathiesen BV, Clausen LR, Skov IR. The role of biomass gasification in low-carbon energy and transport systems. Smart Energy 2021;1:100006. http://dx.doi.org/10.1016/j.segy.2021.100006.

[5] Martinelli M, Gnanamani MK, LeViness S, Jacobs G, Shafer WD. An overview of Fischer-Tropsch synthesis: XtL processes, catalysts and reactors. Appl Catal A 2020;608:117740. http://dx.doi.org/10.1016/j.apcata.2020.117740.

[6] Frazão CJR, Walther T. Syngas and methanol-based biorefinery concepts. Chem Ing Tech 2020;92(11):1680–99. http://dx.doi.org/10.1002/cite.202000108.

[7] Knapczyk A, Francik S, Jewiarz M, Zawiślak A, Francik R. Thermal treatment of biomass: A bibliometric analysis—The torrefaction case. Energies 2021;14(1). http://dx.doi.org/10.3390/en14010162.

[8] Poluzzi A, Guandalini G, d'Amore F, Romano MC. The potential of power and biomass-to-x systems in the decarbonization challenge: a critical review. Curr Sustain Renew Energy Rep 2021;8:242–52. http://dx.doi.org/10.1007/s40518-021-00191-7.

[9] Dossow M, Dieterich V, Hanel A, Spliethoff H, Fendt S. Improving carbon efficiency for an advanced biomass-to-liquid process using hydrogen and oxygen from electrolysis. Renew Sustain Energy Rev 2021;152:111670. http://dx.doi.org/10.1016/j.rser.2021.111670.

[10] Anghilante R, Müller C, Schmid M, Colomar D, Ortloff F, Spörl R, Brisse A, Graf F. Innovative power-to-gas plant concepts for upgrading of gasification biosyngas through steam electrolysis and catalytic methanation. Energy Convers Manage 2019;183:462–73. http://dx.doi.org/10.1016/j.enconman.2018.12.101.

[11] König A, Ulonska K, Mitsos A, Viell J. Optimal applications and combinations of renewable fuel production from biomass and electricity. Energy Fuels 2019;33(2):1659–72. http://dx.doi.org/10.1021/acs.energyfuels.8b03790.

[12] Materazzi M, Holt A. Experimental analysis and preliminary assessment of an integrated thermochemical process for production of low-molecular weight biofuels from municipal solid waste (MSW). Renew Energy 2019;143:663–78. http://dx.doi.org/10.1016/j.renene.2019.05.027.

[13] Ostadi M, Paso KG, Rodriguez-Fabia S, Øi LE, Manenti F, Hillestad M. Process integration of green hydrogen: Decarbonization of chemical industries. Energies 2020;13(18). http://dx.doi.org/10.3390/en13184859.

[14] Butera G, Fendt S, Jensen SH, Ahrenfeldt J, Clausen LR. Flexible methanol production units coupling solid oxide cells and thermochemical biomass conversion via different gasification technologies. Energy 2020;208:118432. http://dx.doi.org/10.1016/j.energy.2020.118432.

[15] Lonis F, Tola V, Cau G. Assessment of integrated energy systems for the production and use of renewable methanol by water electrolysis and CO_2 hydrogenation. Fuel 2021;285:119160. http://dx.doi.org/10.1016/j.fuel.2020.119160.

[16] Kung KS, Thengane SK, Lim CJ, Sokhansanj S, Ghoniem AF. Thermal loss analysis and improvements for biomass conversion reactors. Energy Convers Manage 2020;218:112924. http://dx.doi.org/10.1016/j.enconman.2020.112924.

[17] Ostadi M, Rytter E, Hillestad M. Boosting carbon efficiency of the biomass to liquid process with hydrogen from power: The effect of H_2/CO ratio to the Fischer-Tropsch reactors on the production and power consumption. Biomass Bioenergy 2019;127:105282. http://dx.doi.org/10.1016/j.biombioe.2019.105282.

[18] Marchese M, Buffo G, Santarelli M, Lanzini A. CO_2 from direct air capture as carbon feedstock for Fischer-Tropsch chemicals and fuels: Energy and economic analysis. J CO2 Util 2021;46:101487. http://dx.doi.org/10.1016/j.jcou.2021.101487.

[19] Ostadi M, Austbø B, Hillestad M. Parametric optimization of a power and biomass to liquid process. In: Muñoz SG, Laird CD, Realff MJ, editors. Proceedings of the 9th international conference on foundations of computer-aided process design. Comput aided chem eng, vol. 47, Elsevier; 2019, p. 287–92. http://dx.doi.org/10.1016/B978-0-12-818597-1.50045-X.

[20] Dietrich R-U, Albrecht FG, Maier S, König DH, Estelmann S, Adelung S, Bealu Z, Seitz A. Cost calculations for three different approaches of biofuel production using biomass, electricity and CO_2. Biomass Bioenergy 2018;111:165–73. http://dx.doi.org/10.1016/j.biombioe.2017.07.006.

[21] Guimarães HR, Bressanin JM, Motta IL, Chagas MF, Klein BC, Bonomi A, Filho RM, Watanabe MDB. Bottlenecks and potentials for the gasification of lignocellulosic biomasses and Fischer-Tropsch synthesis: A case study on the production of advanced liquid biofuels in Brazil. Energy Convers Manage 2021;245:114629. http://dx.doi.org/10.1016/j.enconman.2021.114629.

[22] Marchese M, Chesta S, Santarelli M, Lanzini A. Techno-economic feasibility of a biomass-to-x plant: Fischer-tropsch wax synthesis from digestate gasification. Energy 2021;228:120581. http://dx.doi.org/10.1016/j.energy.2021.120581.

[23] Isaacs SA, Staples MD, Allroggen F, Mallapragada DS, Falter CP, Barrett SRH. Environmental and economic performance of hybrid power-to-liquid and biomass-to-liquid fuel production in the United States. Environ Sci Technol 2021;55(12):8247–57. http://dx.doi.org/10.1021/acs.est.0c07674.

[24] Patterson BD, Mo F, Borgschulte A, Hillestad M, Joos F, Kristiansen T, Sunde S, van Bokhoven JA. Renewable CO_2 recycling and synthetic fuel production in a marine environment. Proc Natl Acad Sci 2019;116(25):12212–9. http://dx.doi.org/10.1073/pnas.1902335116.

[25] Ostadi M, Gençer E, Hillestad M. Integration of green power in a gas to liquid process. In: Türkay M, Gani R, editors. 31st European symposium on computer aided process engineering. Comput aided chem eng, vol. 50, Elsevier; 2021, p. 1677–82. http://dx.doi.org/10.1016/B978-0-323-88506-5.50260-6.

[26] Bachmann M, Kätelhön A, Winter B, Meys R, Müller LJ, Bardow A. Renewable carbon feedstock for polymers: environmental benefits from synergistic use of biomass and CO_2. Faraday Discuss 2021;230:227–46. http://dx.doi.org/10.1039/D0FD00134A.

[27] Poluzzi A, Guandalini G, Romano MC. "Potential carbon efficiency" as a new index to track the performance of biofuels production processes. Biomass Bioenergy 2020;142:105618. http://dx.doi.org/10.1016/j.biombioe.2020.105618.

[28] Zhang H, Wang L, Van herle J, Maréchal F, Desideri U. Techno-economic evaluation of biomass-to-fuels with solid-oxide electrolyzer. Appl Energy 2020;270:115113. http://dx.doi.org/10.1016/j.apenergy.2020.115113.

[29] Poluzzi A, Guandalini G, Guffanti S, Elsido C, Moioli S, Huttenhuis P, Rexwinkel G, Martelli E, Groppi G, Romano MC. Flexible power & biomass-to-methanol plants: Design optimization and economic viability of the electrolysis integration. Fuel 2022;310:122113. http://dx.doi.org/10.1016/j.fuel.2021.122113.

[30] Albrecht FG, König DH, Baucks N, Dietrich R-U. A standardized methodology for the techno-economic evaluation of alternative fuels – A case study. Fuel 2017;194:511–26. http://dx.doi.org/10.1016/j.fuel.2016.12.003.

[31] Bernical Q, Joulia X, Noirot-Le Borgne I, Floquet P, Baurens P, Boissonnet G. Sustainability assessment of an integrated high temperature steam electrolysis-enhanced biomass to liquid fuel process. Ind Eng Chem Res 2013;52(22):7189–95. http://dx.doi.org/10.1021/ie302490y.

[32] Ali S, Sørensen K, Nielsen MP. Modeling a novel combined solid oxide electrolysis cell (SOEC) - biomass gasification renewable methanol production system. Renew Energy 2020;154:1025–34. http://dx.doi.org/10.1016/j.renene.2019.12.108.

[33] Singh Aulakh DJ, Boulama KG, Pharoah JG. On the reduction of electric energy consumption in electrolysis: A thermodynamic study. Int J Hydrogen Energy 2021;46(33):17084–96. http://dx.doi.org/10.1016/j.ijhydene.2021.02.161.

[34] Hillestad M, Ostadi M, Alamo Serrano G, Rytter E, Austbø B, Pharoah J, Burheim O. Improving carbon efficiency and profitability of the biomass to liquid process with hydrogen from renewable power. Fuel 2018;234:1431–51. http://dx.doi.org/10.1016/j.fuel.2018.08.004.

[35] Parigi D, Giglio E, Soto A, Santarelli M. Power-to-fuels through carbon dioxide re-utilization and high-temperature electrolysis: A technical and economical comparison between synthetic methanol and methane. J Cleaner Prod 2019;226:679–91. http://dx.doi.org/10.1016/j.jclepro.2019.04.087.

[36] Giglio E, Vitale G, Lanzini A, Santarelli M. Integration between biomass gasification and high-temperature electrolysis for synthetic methane production. Biomass Bioenergy 2021;148:106017. http://dx.doi.org/10.1016/j.biombioe.2021.106017.

[37] Marchese M, Giglio E, Santarelli M, Lanzini A. Energy performance of power-to-liquid applications integrating biogas upgrading, reverse water gas shift, solid oxide electrolysis and Fischer-Tropsch technologies. Energy Convers Manage 2020;6:100041. http://dx.doi.org/10.1016/j.ecmx.2020.100041.

[38] Burheim OS. Engineering energy storage. 1st ed.. Academic Press, Elsevier; 2017.

[39] Graves C, Ebbesen SD, Mogensen M, Lackner KS. Sustainable hydrocarbon fuels by recycling CO_2 and H_2O with renewable or nuclear energy. Renew Sustain Energy Rev 2011;15(1):1–23. http://dx.doi.org/10.1016/j.rser.2010.07.014.

[40] Hauch A, Küngas R, Blennow P, Hansen AB, Hansen JB, Mathiesen BV, Mogensen MB. Recent advances in solid oxide cell technology for electrolysis. Science 2020;370(6513):eaba6118. http://dx.doi.org/10.1126/science.aba6118.
[41] Pham A-Q, Wallman PH, Glass RS. Natural gas-assisted steam electrolyzer. 2000, US Patent 6,051,125.
[42] Martinez-Frias J, Pham A-Q, Aceves SM. A natural gas-assisted steam electrolyzer for high-efficiency production of hydrogen. Int J Hydrogen Energy 2003;28(5):483–90. http://dx.doi.org/10.1016/S0360-3199(02)00135-0.
[43] Wang Y, Liu T, Fang S, Xiao G, Wang H, Chen F. A novel clean and effective syngas production system based on partial oxidation of methane assisted solid oxide co-electrolysis process. J Power Sources 2015;277:261–7. http://dx.doi.org/10.1016/j.jpowsour.2014.11.092.
[44] Tao G, Butler B, Virkar A. Hydrogen and power by fuel-assisted electrolysis using solid oxide fuel cells. ECS Trans 2011;35(1):2929–39.
[45] Wang W, Vohs JM, Gorte RJ. Hydrogen production via CH_4 and CO assisted steam electrolysis. Top Catal 2007;46:380–5. http://dx.doi.org/10.1007/s11244-007-9005-8.
[46] Lee K-J, Lee M-J, Hwang H. High-temperature steam electrolysis combined with methane partial oxidation by solid oxide electrolyzer cells. Appl Surf Sci 2019;473:746–9. http://dx.doi.org/10.1016/j.apsusc.2018.12.128.
[47] Wang Y, Xu J, Meng X, Liu T, Chen F. Ni infiltrated $Sr_2Fe_{1.5}Mo_{0.5}O_{6-\delta}$-$Ce_{0.8}Sm_{0.2}O_{1.9}$ electrode for methane assisted steam electrolysis process. Electrochem Commun 2017;79:63–7. http://dx.doi.org/10.1016/j.elecom.2017.04.018.
[48] Cinti G, Bidini G, Hemmes K. An experimental investigation of fuel assisted electrolysis as a function of fuel and reactant utilization. Int J Hydrogen Energy 2016;41(28):11857–67. http://dx.doi.org/10.1016/j.ijhydene.2016.05.205.
[49] Wang W, Gorte RJ, Vohs JM. Analysis of the performance of the electrodes in a natural gas assisted steam electrolysis cell. Chem Eng Sci 2008;63(3):765–9. http://dx.doi.org/10.1016/j.ces.2007.10.026.
[50] Xu H, Chen B, Ni M. Modeling of direct carbon-assisted solid oxide electrolysis cell (SOEC) for syngas production at two different electrodes. J Electrochem Soc 2016;163(11):F3029–35. http://dx.doi.org/10.1149/2.0041611jes.
[51] Patcharavorachot Y, Thongdee S, Saebea D, Authayanun S, Arpornwichanop A. Performance comparison of solid oxide steam electrolysis cells with/without the addition of methane. Energy Convers Manage 2016;120:274–86. http://dx.doi.org/10.1016/j.enconman.2016.04.100.
[52] Xu H, Chen B, Irvine J, Ni M. Modeling of CH_4-assisted SOEC for H_2O/CO_2 co-electrolysis. Int J Hydrogen Energy 2016;41(47):21839–49. http://dx.doi.org/10.1016/j.ijhydene.2016.10.026.
[53] Luo Y, Shi Y, Li W, Ni M, Cai N. Elementary reaction modeling and experimental characterization of solid oxide fuel-assisted steam electrolysis cells. Int J Hydrogen Energy 2014;39(20):10359–73. http://dx.doi.org/10.1016/j.ijhydene.2014.05.018.
[54] Xu H, Maroto-Valer MM, Ni M, Cao J, Xuan J. Low carbon fuel production from combined solid oxide CO_2 co-electrolysis and Fischer-Tropsch synthesis system: A modelling study. Appl Energy 2019;242:911–8. http://dx.doi.org/10.1016/j.apenergy.2019.03.145.
[55] Xu H, Maroto-Valer MM, Ni M, Cao J, Xuan J. Modeling of a combined CH_4-assisted solid oxide co-electrolysis and Fischer-Tropsch synthesis system for low-carbon fuel production. Energy Procedia 2019;158:1666–71. http://dx.doi.org/10.1016/j.egypro.2019.01.388, Innovative Solutions for Energy Transitions.
[56] Weber A, Ivers-Tiffée E. Materials and concepts for solid oxide fuel cells (SOFCs) in stationary and mobile applications. J Power Sources 2004;127(1):273–83. http://dx.doi.org/10.1016/j.jpowsour.2003.09.024.
[57] Liu T, Liu H, Zhang X, Lei L, Zhang Y, Yuan Z, Chen F, Wang Y. A robust solid oxide electrolyzer for highly efficient electrochemical reforming of methane and steam. J Mater Chem A 2019;7:13550–8. http://dx.doi.org/10.1039/C9TA00467J.